Alberto F. Maroto[1,2,3], Mireia Borrajo[1,2,3], Sílvia Prades[1], Àngela Callejo[4,5], Emilio Amilibia[4,5], Marta Pérez-Grau[4,5], Francesc Roca-Ribas[4,5], Elisabeth Castellanos[5,6], Alejandro Barrallo-Gimeno[1,2,3], Jordi Llorens[1,2,3]

The vestibular calyceal junction is dismantled following subchronic streptomycin in rats and sensory epithelium stress in humans

[1] Departament de Ciències Fisiològiques, Universitat de Barcelona (UB), Feixa Llarga s/n, 08907 l'Hospitalet de Llobregat, Catalunya, Spain.

[2] Institut de Neurociències, Universitat de Barcelona (UB), Barcelona, Catalunya, Spain.

[3] Institut d'Investigació Biomèdica de Bellvitge (IDIBELL), 08907 l'Hospitalet de Llobregat, Catalunya, Spain.

[4] Servei d'Otorinolaringologia, Hospital Universitari Germans Trias i Pujol, Badalona, Catalunya, Spain.

[5] CSUR Phakomatoses Multidisciplinary Clinics HUGTIP-ICO-IGTP, Barcelona, Catalunya, Spain.

[6] Clinical Genomics Research Group, Institut de Recerca Germans Trias i Pujol (IGTP), Badalona, Catalunya, Spain.

Corresponding author: Prof. Jordi Llorens, Ph.D.; e-mail: jllorens@ub.edu; Ph: +34934024277

E-mail addresses and ORCID codes:

A.F.M.: albertomaroto@hotmail.com; 0000-0001-8265-4902

M.B.: mborrajoarjona@ub.edu; 0000-0003-2126-5713

S.P.: silvia.prab@gmail.com; 0000-0001-8561-2919

A.C.: angelacallejo@gmail.com; 0000-0003-3820-7405

E.A.: emilioamilibia@gmail.com; 0000-0003-0587-7891

M.P.G.: martaperezgrau@gmail.com; 0000-0003-4630-0116

F. R.R.: francescrocaribas@gmail.com; 0000-0001-6620-8216

E.C.: ecastellanos@igtp.cat; 0000-0002-8133-5325

A.B.G.: abarrallo@ub.edu; 0000-0003-2086-8926

J.L.: jllorens@ub.edu; 0000-0002-3894-9401

Acknowledgements

This study was supported by grant number RTI2018-096452-B-I00 and PID2021-124678OB-I00 (Ministerio de Ciencia e Innovación, Agencia Estatal de Investigación, MCIU/AEI, 10.13039/501100011033, and European Regional Development Fund, FEDER), grant number 2017SGR621 (Agència de Gestió d'Ajuts Universitaris i de Recerca, AGAUR, Generalitat de Catalunya), and grant number 202007-30-31 (Fundació La Marató de TV3 2019) . A.B.G is a Serra-Húnter fellow. The electron and confocal microscopy studies were performed at the Centres Científics i Tecnològics de la UB (CCiTUB) of the Universitat de Barcelona. We thank Benjamín Torrejon-Escribano, Rosa Rivera, Adriana Martínez Gené, Mora Gimeno, Josep Manel Rebled and Eva Prats for the expert and technical help. We also thank Dr Bechara Kachar for the generous gift of the KCNQ4 antibody and Dr. Erin A. Greguske for revision of the manuscript. We are also grateful to the patients that gave consent to the research use of their sensory tissues.

Competing interests: The authors declare no competing interests

ABSTRACT

Hair cell (HC) loss by epithelial extrusion has been described to occur in the rodent vestibular system during chronic 3,3'-iminodipropionitrile (IDPN) ototoxicity. This is preceded by dismantlement of the calyceal junction in the contact between type I HC (HCI) and calyx afferent terminals. Here, we evaluated whether these phenomena have wider significance. First, we studied rats receiving streptomycin for 3 to 8 weeks. Streptomycin caused loss of vestibular function associated with partial loss of HCI and decreased expression of contactin-associated protein (CASPR1), denoting calyceal junction dismantlement, in the calyces encasing the surviving HCI. Additional molecular and ultrastructural data supported the conclusion that HC-calyx detachment precede HCI loss by extrusion. Animals allowed to survive after the treatment showed functional recuperation and rebuilding of the calyceal junction. Second, we evaluated human sensory epithelia obtained during therapeutic labyrinthectomies and trans-labyrinthine tumour excisions. Some samples showed abnormal CASPR1 label strongly suggestive of calyceal junction dismantlement. Therefore, reversible dismantlement of the vestibular calyceal junction may be a common response triggered by chronic stress, including ototoxic stress, before HCI loss. This may partly explain clinical observations of reversion in function loss after aminoglycoside exposure.

54 **INTRODUCTION**

55 Sensory encoding by the inner ear's vestibular system depends on the transducing function of hair cells (HC). In
56 most mammals, permanent loss of equilibrium and gaze control occurs as a result of HC loss considering that
57 these cells do not regenerate to a significant extent to restore functionality. Nevertheless, significant
58 recuperation in vestibular function is recorded clinically in a variety of disease conditions. In some cases, such as
59 benign paroxysmal positional vertigo (von Brevern et al., 2015), recuperation can be complete, suggesting that
60 the condition is associated with pathogenic mechanisms that transiently impair the system's function, but do
61 not cause HC loss. In other disease conditions, such as Ménière's disease (López-Escámez et al., 2015), recurrent
62 crises are often associated with incomplete recuperation and progressive worsening of the vestibular function.
63 In the case of exposure to ototoxic aminoglycoside antibiotics, irreversible loss of vestibular function is a
64 common outcome (Black et al., 2004), but significant yet incomplete recuperation has also been recorded (Black
65 et al., 2001). In recent years, we have used a sub-chronic ototoxicity model to identify reversible cellular and
66 molecular alterations in the vestibular epithelia that associate with reversible loss of vestibular function in rats
67 (Sedó-Cabezón et al., 2015) and mice (Greguske et al., 2019). These studies showed that the sub-chronic
68 ototoxic stress caused by the experimental compound 3,3'-iminodipropionitrile (IDPN) results in the
69 dismantlement of the calyceal junction between type I HCs (HCI) and the calyx afferent terminals, as
70 demonstrated by ultrastructural characterization and observed loss of the junction proteins CASPR1 (contactin-
71 associated protein) and tenascin-C, as well as delocalization of the voltage-gated potassium channel KCNQ4.
72 Simultaneously, the vestibular epithelium showed a loss of pre-synaptic and post-synaptic proteins, indicative of
73 synaptic uncoupling between the HCs and their afferents. These changes that are associated with the loss of
74 vestibular function are revealed by visible behavioural deficits. In this model, if the exposure was halted at an
75 early stage of the toxicity, both the epithelium alterations and the behavioural dysfunction were largely
76 reversible. In contrast, if the exposure was maintained, the functional loss persisted as a result of HC loss, which

77 predominantly occurred by the extrusion of live cells from the sensory epithelium into the endolymphatic cavity
78 (Llorens and Rodríguez-Farré, 1997; Seoane et al., 2001a,b; Sedó-Cabezón et al., 2015; Greguske et al., 2019).

79 The rat and mouse sub-chronic IDPN models illustrate a cellular pathway to HC demise that differs from
80 apoptosis (Seoane et al., 2001a). As explained in the previous paragraph, it concludes with the extrusion of HCs
81 after a phase of sensory cell detachment and synaptic uncoupling (Sedó-Cabezón et al., 2015; Greguske et al.,
82 2019). The fact that extrusion is the main form of HC demise in birds and amphibians following a variety of
83 insults (Hirose et al., 1999; Rubel et al., 2013), suggests that its molecular mechanisms may be highly conserved
84 across vertebrates and operate in response to diverse forms of damage. Surprisingly, this phenomenon has
85 received scarce attention and information is lacking about its molecular mechanisms and relevance to human
86 health. One first question worth addressing is whether these phenomena have a role in mammalian
87 aminoglycoside toxicity *in vivo*, as this is the main cause of vestibular toxicity in humans. Although most research
88 on aminoglycoside-induced HC loss has focused on apoptosis (Furness, 2015), the literature also contains
89 evidence that these drugs may cause vestibular HC extrusion (Li et al., 1995; Nakagawa et al., 1997; Granados
90 and Meza, 2005). In the present work, we studied whether dismantlement of the calyceal junction, synaptic
91 uncoupling, and HC extrusion occur in the rat vestibular epithelium in response to one aminoglycoside
92 antibiotic, streptomycin. Previously, we found that the mode of HC demise, whether extrusion, apoptosis, or
93 necrosis was determined by the intensity and duration of the toxic stress. Thus, high acute doses of IDPN caused
94 HC necrosis, sub-acute exposure to medium doses caused HC apoptosis and sub-chronic low dose exposure
95 elicited HC extrusion (Seoane et al., 2001a). These data indicate that short exposure paradigms aimed at
96 accelerating and synchronizing HC demise (Taylor et al., 2008; Oesterle et al., 2008; Benkafadar et al., 2021) may
97 in fact favour the apoptotic pathways above other possible pathways. Accordingly, for the present study we
98 investigated the effects of sub-chronic aminoglycoside exposure. As a second approach to evaluate the
99 relevance of these phenomena to human disease conditions, we explored their occurrence in the vestibular
100 epithelia of a substantial number of patients with vestibular schwannoma and a few with other vestibular

101 diseases that also require trans-labyrinthine tumour excision (meningioma and endolymphatic sac tumour) or
102 therapeutic labyrinthectomy (Ménière's disease). Vestibular schwannomas are tumours that grow in the
103 vestibular nerve and cause hearing and vestibular function loss. Current evidence indicates that this loss may in
104 part be caused by the negative impact pro-inflammatory factors secreted by the tumour have on the sensory
105 epithelia (Dilwali et al., 2015). The data we obtained demonstrate that calyceal junction dismantlement occurs
106 during chronic streptomycin toxicity in rats and provide evidence that it occurs in human vestibular epithelia in
107 response to other types of stress.

108 **MATERIALS AND METHODS**

109 **Animals and treatments**

110 Animals were used in accordance with Law 5/1995 and Act 214/1997 of the Generalitat de Catalunya and
111 approved by the University of Barcelona's Ethics Committee on Animal Experiments and the Commission on
112 Animal Experimentation of the Generalitat. Long-Evans rats were obtained from Janvier Labs (Le-Genest-Saint-
113 Isle, France) at post-natal day 8-12. They were housed with lactating mothers in standard Macrolon cages
114 (215×465×145 mm) with wood shavings as bedding. At day 21, the rats were weaned and housed in groups of
115 four of the same sex. Housing conditions included a 12:12 h light:dark cycle (07:30-19:30 h), a 22±2°C room
116 temperature and an *ad libitum* access to standard pellet diets (TEKLAD 2014, Harlan Laboratories, Sant Feliu de
117 Codines, Spain).

118 A total of 98 rats (58 males, 40 females) were used in two different administration protocols, one injection per
119 day and two injections per day. The first administration protocol was designed on the grounds of the protocols
120 by Granados and Meza, 2005, and Schirmer et al., 2007. Animals were administered streptomycin sulphate salt
121 (Sigma-Aldrich, S6501), s.c., dissolved in PBS, starting at postnatal 21, daily for 6 or 8 weeks. To ensure dose
122 accuracy, injection volumes were 10 ml/kg at the beginning, but were reduced to 2 ml/kg as the rats increased
123 body weights. Different injection sites in the dorsal skin were used in an alternating sequence. In this first series
124 of experiments, rats were dosed with 0 (control vehicle), 100, 300, 400 or 500 mg/kg · day of streptomycin
125 (referred to the free base), once a day, for 6 or 8 weeks. Two experimental batches used only males, one of
126 them used only females, and the fourth one included an equal number of males and females. Acute toxicity and
127 lethality is described in the results section above. A final experiment used a second administration protocol, in
128 which the total daily dose was split into two injections given 8 h apart. This dosing paradigm was designed to
129 evaluate the vestibular effects of larger daily doses and circumvent the acute toxicity of streptomycin recorded
130 in rats receiving the 500 mg/kg dose. Thus, rats received 0, 600, 700 or 800 mg/kg · day in two daily doses of 0,

131 300 mg/kg (for 6 weeks), 350 mg/kg (for 4 weeks) or 400 mg/kg (for 3 weeks). No animals died in this
132 experiment. The detail of all groups of animals used is shown in Supplementary Table S1.

133 During the period of treatment, the animals were weighted and assessed for wellbeing daily. They were also
134 tested for vestibular function once a week. At the end of the treatment period, some animals were allowed to
135 survive for up to 8-10 additional weeks to evaluate the potential reversibility of the vestibular dysfunction and
136 the histopathological effects of streptomycin. Some control animals were also allowed to survive the recovery
137 period to provide control body weight and vestibular function data. The day after that of the last dose, or after
138 the recovery period, rats were euthanized by decapitation under anaesthesia. The skull was sectioned in half
139 and placed in fixative solution under a fume hood for dissection of the vestibular sensory epithelia. The epithelia
140 from the first ear were typically obtained within 5 min after decapitation and used for scanning (SEM) and
141 transmission (TEM) electron microscopy. The epithelia from the second ear, obtained within 15 min after
142 decapitation, were used for immunohistochemistry. Epithelia from some animals were used for
143 immunohistochemical analysis only. The numbers of animals used in each histological analysis are indicated in
144 the figures and are summarized in Suppl. Table S2.

145 **Human samples**

146 Vestibular sensory epithelia were collected from patients submitted to therapeutic labyrinthectomy or
147 translabyrinthine tumour excision. The samples included in the study, detailed in Suppl. Table S3, are from 2
148 cases of Ménière's Disease, 1 case of endolymphatic sac tumour, 4 cases of meningioma, and 22 cases of
149 vestibular schwannoma. Patients were 18 to 70 years old, and 52 % were females. The tissues were obtained
150 after informed consent, as approved by the Clinical Ethics Committee of the Hospital Germans Trias i Pujol. The
151 samples were immediately placed in 4% formaldehyde with <2.5% methanol (BiopSafe) and sent to the
152 laboratory, usually in 24 h, although some samples were delayed for up to 7 days (Suppl. Table S3). The tissues

153 were then rinsed in phosphate buffered saline (PBS, pH 7.2), transferred into a cryoprotective solution (34.5%
154 glycerol, 30% ethylene glycol, 20% PBS, 15.5% distilled water) and stored at -20ºC until further processing.

155 **Assessment of vestibular function in rats**

156 To evaluate vestibular function, we assessed the tail-lift reflex as described (Martins-Lopes et al., 2019; Maroto
157 et al., 2021 a,c). Briefly, rats are held by the base of the tail and quickly but gently lifted upwards to
158 approximately 40 cm above ground and immediately returned down. In healthy rats, this triggers a trunk and
159 limbs extension reflex in a landing response. Loss of vestibular function results in loss of the anti-gravity
160 extension reflex, so the rat curls ventrally (Hunt et al., 1987; Pellis et al., 1991; Llorens et al., 1993; Maroto et al.,
161 2021c). The reflex response of the animal is recorded from the side with high-speed video (we use 240 frames
162 per second with a GoPro 5 camera) and the records are used to obtain the minimum angle formed by the nose,
163 the back of the neck and the base of the tail during the tail-lift manoeuvre (tail-lift angle, TLA), as described
164 (Martins-Lopes et al., 2019; Maroto et al., 2021a,c). The TLA has been demonstrated to provide an objective
165 measure of permanent or reversible vestibular loss (Martins-Lopes et al., 2019; Maroto et al., 2021a,c).

166 **Electron microscopy**

167 For SEM and TEM, rat vestibular epithelia were dissected in 2.5% glutaraldehyde in 0.1 M cacodylate buffer (pH
168 7.2), and fixed overnight in this solution. The epithelia were then rinsed with cacodylate buffer, post-fixed for 1
169 h in 1% osmium tetroxide in the same buffer, rinsed again and stored in 70% ethanol at 4ºC until further
170 processing. Afterwards, the samples were dehydrated with increasing concentrations of ethanol, up to 100%.
171 For TEM analysis, the lateral crista was embedded in Spurr resin. To select the level of interest, semi-thin
172 sections (1 µm) were stained with 1% toluidine blue and examined in a light microscope. Ultrathin sections were
173 stained with uranyl acetate and lead citrate and were observed with a JEOL 1010 microscope at 75-80 kV. For
174 SEM analysis of epithelial surfaces, the dehydrated specimens were dried in a Polaron E3000 critical-point dryer
175 using liquid CO2, coated with carbon, and observed in a JEOL JSM-7001F field emission SEM.

176 **Immunohistochemistry**

177 The following commercial primary antibodies were used: mouse monoclonal anti-CASPR1 (clone K65/35, RRID:
178 AB_2083496, used at 1:400 dilution) and anti-PSD95 (clone K28/43, RRID: AB_2292909, 1:100) from the UC
179 Davis / NIH NeuroMab Facility; mouse monoclonal anti-Ribeye/CtBP2 (clone 16/CtBP2, BD Transduction Labs,
180 RRID: AB_399431, 1:100); rabbit anti-myosin VIIa (25-6790, Proteus Biosciences, RRID: AB_10015251; 1:400);
181 guinea pig anti-calretinin (214.104, Synaptic Systems, RRID: AB_10635160, 1/500); goat anti-SPP1 (AF808, RD
182 systems, RRID: AB_2194992, 1/200). We also used a rabbit anti-KCNQ4 (PB-180, 1/1000) donated by Bechara
183 Kachar (National Institute on Deafness and Other Communication Disorders, NIH; Beisel et al., 2005). To reveal
184 the primary antibodies, we used Day-Light-405, Alex-488, Alexa-555 and Alexa-647-conjugated secondary
185 antibodies from Invitrogen / Thermo Fisher. To image synaptic puncta, we used isotype-specific secondary
186 antibodies, i.e., anti-mouse-IgG1 to reveal the Ribeye/CtBP2 antibody and anti-mouse IgG2a to reveal the PSD-
187 95 antibody.

188 After dissection, the rat vestibular epithelia were fixed for 1 h at room temperature in 4 % paraformaldehyde in
189 PBS. These samples were rinsed in PBS, transferred into the cryoprotective solution and stored at -20ºC. To
190 circumvent potential bias from batch-to-batch differences in immunolabelling, we processed in parallel
191 specimens from each experimental group. For immunolabelling, rat or human tissues were washed with PBS to
192 remove the cryoprotective solution, permeated in 4% Triton-X-100 in PBS for 1 h at room temperature, and then
193 blocked in 0.5% Triton-X-100 and 1% fish gelatine in PBS (Sigma-Aldrich, cat.# G7765) also for 1 h at room
194 temperature. They were then incubated with the mixed primary antibodies in 0.1% Triton-X-100 and 1% fish
195 gelatine in PBS for 24 h at 4ºC, followed by incubation with the secondary antibodies in the same conditions
196 (Lysakowski et al., 2011). The samples were thoroughly rinsed with PBS following each incubation and gently
197 rocked during the incubations and washes. The immunolabelled human epithelia were whole-mounted in
198 Mowiol medium, whereas the rat epithelia were sectioned before mounting in the same medium. To obtain
199 sections, the tissues were embedded in a mixture of 0.49% gelatin, 30% bovine serum albumin, and 20% sucrose

200 in PBS overnight at 4 ºC. This same medium was used to form a block by solidification with 2 % glutaraldehyde,
201 one sample placed oriented in its surface, and a second block formed on top of it. Using a Leica VT1000S
202 vibrating microtome, sections of 40 μm were obtained from this layered block with the specimen placed in
203 between the two halves. A detailed version of this protocol has been published (Maroto et al., 2021b).

204 **Confocal microscopy observation and analysis**

205 Tissue sections were observed in a Zeiss LSM880 spectral confocal microscope. In animal studies, image
206 acquisition settings were maintained across samples from each immunolabelling batch. To obtain HC counts, Z-
207 stacks of optical sections were obtained each 0.5 μm spanning 25 μm with a 63X objective. Then, we obtained 8
208 sequential images (3 μm thick each) by the maximum intensity projection of 6 consecutive images from the
209 original stack. The ImageJ software (National Institute of Mental Health, Bethesda, Maryland, USA) was used for
210 quantitative image analyses. Epithelia of animals injected once a day with streptomycin were labelled with anti-
211 MYO7A, anti-CASPR1, and anti-calretinin antibodies. HCI were defined as MYO7A+ cells surrounded by a calyceal
212 CASPR1+ label, even in cases where this label appeared thin and fragmented, or cells with an unambiguous HCI
213 shape with a long and narrow neck. HCII were defined as cells labelled with both the anti-MYO7A and anti-
214 calretinin antibodies. MYO7A+ cells not identified as HCI or HCII (3-6 %) were excluded from the analysis. For
215 each animal and epithelial zone, a representative count of HCI and HCII was obtained by averaging counts from
216 images 1, 4 and 7 from the series of 8 sequential images generated from a representative histological section.
217 The histological sections used for counting were obtained from similar locations in all animals. To evaluate the
218 loss of CASPR1 label in the calyces, the amount of fluorescence in the corresponding colour channel was
219 measures in individual calyces using a 100 μm^2 region of interest on a single optical section. For each animal,
220 epithelium and zone, the average amount of fluorescence was obtained from all HCs available for analysis up to
221 40 cells. Data were normalized as percentage of the mean fluorescent intensity of control samples in the same
222 batch of immunohistochemical processing and confocal imaging. Then, statistical analyses were performed to

223 compare among groups of animals. To compare the distribution of KCNQ4 in the inner and outer membranes of
224 the calyx, we assessed the profile of fluorescence intensity along a line drawn across the calyx as described
225 (Sousa et al., 2009; Sedó-Cabezón et al., 2015). Peak fluorescence values were obtained for the inner and outer
226 membrane of all calyces included in one representative section of the epithelium, and average values were
227 obtained per animal. To count synaptic puncta, we imaged the tissues at 0.3 μm intervals to obtain Z-stacks of
228 2.7 μm. Only HC with their nuclei extending top to bottom of the stack were used for counting, so the counts
229 obtained were from a thick slice from the middle region of the cell, not the whole cell. We counted presynaptic
230 Ribeye/CtBP2 puncta, postsynaptic PSD95 puncta, and pairs of Ribeye and PSD95 puncta that overlapped or
231 were closely apposed (co-localization). For each animal, average counts were obtained from a minimum of 30
232 HC.

233 Human samples were observed as whole mounts. The tissues were completely examined with 40X and 63X
234 objectives. Representative Z-stacks, encompassing the entire thickness of the sensory epithelium, were obtained
235 from both striola and peripheral regions. The full stacks were thoroughly studied to determine the presence of
236 pathological features. This included colour channel splitting and merging, observation at several different
237 contrast and brightness adjustments, 3D reconstructions, maximum intensity projection of stacks or sub-stacks
238 and orthogonal projections. Images in Fig. 10 were prepared for illustration purposes only.

239 **Data analysis**

240 Data show mean +/- standard error of the mean except where indicated. Body weight and behavioural data
241 were analysed with repeated-measures MANOVA (Wilks' criterion) with the day as the within-subject factor.
242 Day-by-day analysis was performed after significant day-by treatment interactions were recorded. Other data
243 were analysed by appropriate ANOVA designs and Duncan's post-hoc test, or by Student's t-test. The IBM SPSS
244 Statistics 25 program package was used.

245

246 **RESULTS**

247 **Effects of streptomycin sulphate on body weight and overall health.**

248 To study the sub-chronic toxicity of streptomycin on the vestibular system, we administered male and female
249 rats with one daily dose of streptomycin sulphate (0, 100, 300, 400 or 500 mg/kg x day - groups CTRL, STR-100,
250 STR-300, STR-400, STR-500) for up to 6 or 8 weeks, starting at day 21 of age. Other groups of rats were
251 administered with two daily doses of 0, 300, 350 or 400 mg/kg - groups CTRL, STR-300x2, STR-350x2, STR-
252 400x2). Rats administered with streptomycin showed an acute sedative effect starting within a few minutes
253 after each daily dose, and was most evident in the group receiving the highest dose (STR-500): the animal stayed
254 quiet with decreased responsiveness and with an overtly low muscle tone. This effect usually lasted 15-20 min
255 but sometimes lasted for up to two hours after injection. During this sedation period, two rats died in the STR-
256 500 group on days 5 and 36, likely from respiratory arrest. Additionally, two rats died for unknown reasons after
257 days 20 and 37 in the STR-300 and STR-500 groups, respectively. No animals died when larger daily doses were
258 administered via two daily injections. Recuperation from this sedative effect was complete and surviving animals
259 showed normal behaviour except in regards to the evidences of vestibular dysfunction explained below. As
260 shown in Suppl. Fig. S1, streptomycin animals showed an increase in body weight at a smaller rate than that
261 shown by control rats. This resulted in significant differences in streptomycin versus control body weights after
262 five or more weeks of one daily dose, and by two weeks in the groups receiving two daily doses.

263 **Loss and recuperation of vestibular function after sub-chronic streptomycin exposure.**

264 Sub-chronic exposure to streptomycin sulphate caused a dose-dependent loss of vestibular function, as
265 indicated by the rat's abnormalities in spontaneous motor behaviour. Vestibular deficient animals showed
266 ataxia, spontaneous circling, and head bobbing. The loss of function was assessed using high-speed video
267 records of the tail-lift reflex as described (Martins-Lopes et al., 2019; Maroto et al., 2021a,c). A similar dose-
268 dependent effect occurred in male and female animals (Suppl. Fig. S2), and therefore animals of both sexes

269 were pooled for all further analyses. The decrease in tail-lift angles, indicative of loss of vestibular function, was
270 not significant in the STR-100 group, and smaller in the STR-300 and STR-400 groups compared to the STR-500
271 group (Suppl. Fig. S3), so further analysis on the one daily dose paradigm focused on the 500 mg/kg x day dose
272 level. As shown in Figure 1A, a progressive reduction in tail-lift angles was recorded in the STR-500 rats.
273 Repeated-measures MANOVA of the tail-lift data from days 0 (pre-test) to 42 resulted in significant day
274 ($F[6,28]=15.38$, $p<0.001$), treatment ($F[1,33]=18.0$, $p<0.001$), and day X treatment interaction ($F[6,28]=9.766$,
275 $p<0.001$) effects, with significant differences between CTRL and STR-500 mean values recorded at 4 to 6 weeks
276 of exposure. Extension of the administration up to 8 weeks caused only a modest additional effect on vestibular
277 function (Suppl. Fig. S4A).

278 By administering streptomycin in two daily injections, larger doses could be given to the animals and circumvent
279 the risk of death associated with the acute sedative effects of the drug. As shown in Fig. 1B, all the STR-300x2,
280 STR-350x2, and STR-400x2 groups showed faster and deeper loss of vestibular function than the STR-500 group
281 (Fig. 1A). MANOVA of the tail-lift data from the two daily injections experiment up to day 21 resulted in
282 significant day ($F[3,26]=191.1$, $p<0.001$), treatment ($F[3,28]=45.89$, $p<0.001$), and day X treatment interaction
283 ($F[9,63.4]=20.92$, $p<0.001$) effects. The effect was dose-dependent, and larger doses caused a faster progression
284 of the decline in vestibular function.

285 To evaluate the potential for functional recuperation, some animals were allowed to survive after the end of the
286 sub-chronic streptomycin exposure. As shown in Fig. 1C, rats exposed to 500 mg/kg · day of streptomycin for 6
287 weeks regained normal tail-lift angles during the recovery period. Functional recuperation was also observed in
288 the STR-500 rats exposed for 8 weeks (Suppl. Fig. S4B). The individual values of animals allowed to recover after
289 3 weeks of two daily doses of streptomycin also showed a clear recuperation of the tail-lift reflex (Fig. 1D).

290 **Sub-chronic streptomycin exposure caused partial loss of HCs in the vestibular sensory epithelia.**

291 To evaluate the major effects of streptomycin on the vestibule, we observed surface preparations of the sensory
292 epithelia using scanning electron microscopy (SEM). As reported in previous studies (Llorens et al., 1993; Seoane
293 et al., 2001a; Sedó-Cabezón et al., 2015), SEM observation of control epithelia (n=16) (Fig. 2A; Suppl. Fig. S5A, B)
294 revealed morphological features matching literature descriptions of healthy untreated rats with high densities of
295 stereocilia bundles. Epithelia from STR-300 animals (6 weeks of exposure, n=3) showed similar features to
296 control epithelia, except for indications of a few missing hair bundles or occasional bundles with fused
297 stereocilia (data not shown). For animals administered with larger doses of streptomycin once a day, the SEM
298 observations revealed scant to moderate loss of stereocilia bundles. Similar findings were obtained in STR-500
299 rats with small difference observed between animals exposed for 6 (n=6) or 8 (n=7) weeks, and in STR-400 rats
300 exposed for 8 weeks (n=2). Hair bundle loss was roughly similar in cristae (Suppl. Fig. S5C), utricles (Suppl. Fig.
301 S5D), and saccules (Fig 2B, C), with no evidence of an overt difference in susceptibility among receptors. In all
302 cases, the loss of stereocilia bundles was partial and many bundles were still present in the sensory receptors of
303 the worst cases (Suppl. Fig. S5E,F). In these SEM observations, images indicating ongoing damage were scarce.
304 Nevertheless, some evidence for fused stereocilia and HC protrusion were found (Fig 2D,E). Animals given two
305 daily injections of streptomycin displayed a larger loss of stereocilia bundles than the animals administered for
306 once a day (Suppl. Fig. S6). Evidence for ongoing damage was scarce in some epithelia, but clear in other
307 samples, including images of epithelial scars, bundle fusion, and cell protrusion towards the endolymphatic
308 cavity (Suppl. Fig. S6). The average extent of hair bundle loss was similar in STR-300x2 rats treated for 6 weeks
309 (n=7), STR-350x2 rats treated for 4 weeks (n=6), and STR-400x2 rats treated for 3 weeks (n=6).

310 To determine the loss of HCs revealed by the decreased densities of hair bundles observed by SEM in STR-500
311 rats, we obtained type I HC (HCI) and type II HC (HCII) counts from the vestibular epithelia of the other ear of the
312 same animals. To this end, we immunostained the epithelia with antibodies against myosin-7a (MYO7A),
313 CASPR1, and the calcium-binding protein calretinin, revealed by fluorescent secondary antibodies. In the
314 confocal microscopy images, HCI were identified as MYO7A+ cells (a pan-HC marker, Hasson et al., 1997)

315 surrounded by a CASPR1+ calyx (Sousa et al., 2009; Lysakowski et al., 2011; Sedó-Cabezón et al., 2015), even if
316 weak or fragmented, or with an unambiguous HCI shape with a long and narrow neck. As an estimate of HCII, we
317 counted cells with double MYO7A and calretinin label (Dechesne et al., 1991). The data obtained, presented in
318 Fig. 3A-C, reveal a significant decrease in HCI counts in the central region of the crista, in both the centre and
319 periphery of the utricle and in the periphery of the saccule. ANOVA results were: central crista, $F[3,27]= 11.95$,
320 $p<0.001$; peripheral crista, $F[3,24]=2.76$, $p=0.064$; central utricle, $F[3,25]=17.36$, $p<0.001$; peripheral utricle,
321 $F[3,26]=23.51$, $p<0.001$; central saccule, $F[3,20]=1.68$, $p=0.20$ - N.S.; peripheral saccule, $F[3,22]=9.08$, $p=0.001$.
322 The most affected receptor was the utricle with a 52-67 % decrease in HCI counts in STR-500 animals, followed
323 by the crista, where a 30-40 % loss was recorded. In both the crista and the utricle, similar effects were recorded
324 in animals exposed for 6 weeks and animals exposed for 8 weeks. In the saccule, the loss was smaller than in the
325 crista and utricle receptors, and greater at 8 weeks than at 6 weeks of treatment. HCI counts remained reduced
326 in animals allowed to recover after the end of the exposure period, indicating an insignificant capacity for
327 regeneration. In contrast to HCI, no significant differences were obtained among treatment groups in HCII
328 counts (all p values > 0.1).

329 As explained above, the SEM observations indicated a loss of HC after two daily injections of streptomycin
330 greater than that recorded after one daily injection. To estimate HC loss according to cell type, we
331 immunostained crista receptors with antibodies against secreted phosphoprotein 1 (SPP1) / osteopontin,
332 CASPR1, and calretinin. HCI were identified by the SPP1 label (Burns et al., 2015; McInturff et al., 2018; Maroto
333 et al., 2021b), while the main population of HCII was identified by the calretinin+ label. As shown in Fig. 3D,E,
334 the number of HCI was greatly reduced after two daily injections of streptomycin ($F[4,26]=77.64$; $p<0.001$), while
335 the number of HCII was unchanged ($F[4,26]=1.48$, $p=0.24$). The loss of HCI was similar in the three groups of rats
336 treated with streptomycin (STR-300x2, STR-350x2, STR-400x2), and no recuperation in HCI counts was recorded
337 in the recovery group.

338 **Calyceal junction dismantlement, afferent fragmentation, and synaptic loss after sub-chronic streptomycin**
339 **exposure.**

340 In addition to HCl loss, rats exposed to sub-chronic streptomycin displayed alterations in the remaining HCIs and
341 their afferents. In rats exposed to streptomycin once a day (STR-500), a reversible loss of CASPR1 fluorescence
342 occurred in the calyces contacting the surviving HCIs (Fig.5). To assess this effect, we measured the amount of
343 CASPR1 fluorescence associated with the remaining individual calyces. The loss and recuperation of the CASPR1
344 label was found across the three epithelia and in both central/striolar and peripheral zones. All ANOVA
345 comparisons resulted in significant differences (all $F[3, 19 \text{ to } 27] > 5.3$, all $p's<0.006$). As shown in Fig. 4, the
346 confocal microscope images also revealed a reversible decrease in MYO7A fluorescence intensity in the HCs of
347 the STR-500 animals. This effect was quantified in a subset of samples and significant group differences were
348 found ($F[2,11]=5.0$, $p=0.029$). The post-hoc analysis confirmed that the label (in arbitrary units) was reduced
349 from 9583 $\pm$ 1290 ($X\pm SE$, n=5) in CTRL animals to 6232 $\pm$ 781 (n=4) in STR-500 (8 wk) animals ($p<0.05$, Duncan's
350 test), and regained normal level (10522 $\pm$ 621, n=5) after recovery. In animals given two injections a day, the
351 intensity of CASPR1 immunoreactivity in the calyces contacting surviving HCI was also reduced by streptomycin
352 (Suppl. Fig. S7).

353 We also evaluated whether sub-chronic streptomycin altered the distribution of the potassium channel, KCNQ4,
354 in the calyx membrane, as identified in CASP1-KO mice (Sousa et al., 2009) and in rats exposed to sub-chronic
355 IDPN (Sedó-Cabezón et al., 2015). The data, shown in Fig. 5A,B, indicated that CASPR1 loss is associated with
356 KCNQ4 redistribution in the calyces of the STR-500 rats. In control rats, the KCNQ4 label is found almost
357 exclusively in the inner membrane, that is, in the calyceal junction area, and is absent in the outer membrane of
358 the calyx. After streptomycin treatment, the immunofluorescence was reduced in the inner membrane, whereas
359 significant labelling appeared in the outer membrane of the calyx. Therefore, KCNQ4 was abnormally distributed
360 after streptomycin. ANOVA analyses of the amount of fluorescence in the inner and outer membranes were

361 significant ($F[3, 14]=12.1$, $P<0.001$, and $F[3,14]=49.9$, $p<0.001$, respectively). Post-hoc analyses confirmed that
362 streptomycin caused KCNQ4 redistribution, and that this effect was no longer present in the recovery animals.

363 Sub-chronic streptomycin also caused a reduction in the number of synaptic puncta as revealed by labelling with
364 antibodies against ribeye/CtBP2, the core protein of the presynaptic ribbon, and against the post-synaptic
365 scaffold protein PSD-95 (post-synaptic density 95). The mean number of puncta counts per cell in 2.7 μm thick
366 sections of HCs was significantly reduced in STR-500 animals exposed for 6 weeks compared to CTRL animals
367 (Fig. 5C,D). T-test comparisons resulted in $p <0.001$, $p=0.018$, and $p=0.001$ for ribeye, PSD-95, and co-localization
368 (as defined in the methods section) values, respectively.

369 The effect of sub-chronic streptomycin on the calyceal junction was also studied at the ultrastructural level by
370 TEM observation of samples from control rats (4 lateral crista, 2 saccules, 1 utricle), STR-500 rats exposed for 6
371 (5 lateral crista) or 8 (4 lateral crista) weeks, and STR-300x2 rats exposed for 6 weeks (3 saccules and 1 utricle).
372 In control specimens, calyceal junctions were prominent with virtually no disruptions in the two basal thirds of
373 contact between HCI and its afferent calyx (Fig. 6A,C). This junction consists of highly electron-dense pre- and
374 post-synaptic membranes, a highly regular inter-membrane distance, and an electron-dense extracellular space.
375 In contrast, many calyces in the streptomycin rats showed from fragmented to only partial to absent junctions
376 (Fig. 6B, D-F). In these units, the membrane density was similar to that of regular membranes and the area
377 displayed a more-variable inter-membrane distance, as well as a reduced extracellular electron density. In
378 addition, fragmented calyces were also identified in the samples from the treated animals, and these showed
379 absence of the calyceal junction (Fig. 6E, F). No fragmented calyces were observed in the control epithelia.

380 **Hair cell extrusion after sub-chronic streptomycin exposure.**

381 The occurrence of HC extrusion was evaluated by immunofluorescent analysis in samples from animals exposed
382 to streptomycin twice a day. The MYO7A and CASPR1 antibodies were combined with an anti-radixin antibody to
383 label the apical microvilli of the supporting cells and thus outline the surface of the epithelium. Images indicating

384 HC extrusion were not obtained in most sections of the crista (n=4 CTRL, 7 STR-300x2, 4 STR-350x2, and 4 STR-
385 400x2) and saccule (n=2 CTRL, 7 STR-300x2, 5 STR-350x2, and 6 STR-400x2). However, as illustrated in Fig. 7A,
386 protruding/extruding HCs were a common finding in most utricle sections from animals exposed to STR-300x2
387 for 6 weeks (n=7) or STR-350x2 for 4 weeks (n=5), although not in utricles from animals receiving STR-400x2 for
388 3 weeks (n=6). Control utricles (n=2) also showed no HC extrusion. In the STR-300x2 and STR-350x2 utricles, the
389 occurrence was around 1-3 protruding/extruding HC per section (130-190 μm long, 25 μm thick).

390 To corroborate that the extruding MYO7A+ profiles found in the immunofluorescent analyses corresponded to
391 living HCs, we examined two utricles by TEM. As shown in Fig. 7B,C, the extruding HC showed displacement of
392 the whole cell towards the lumen of the utricle. The ultrastructural features of the cytoplasm, organelles, and
393 nucleus indicated continued activity of the cell.

394 **Occurrence of calyceal junction dismantlement in human vestibular epithelia.**

395 To evaluate whether calyceal junction dismantlement also occurs in human vestibular epithelia under stress, we
396 studied samples from patients submitted to therapeutic labyrinthectomy or translabyrinthine tumour excision.
397 The vestibular epithelia were immunolabeled with anti-CASPR1 antibodies combined with a variety of other
398 antibodies, and a total of 29 samples yielded useful information. MYO7A, calretinin, and CASPR1 labels matched
399 the labelling features described above in rat samples. Also, when tested together (n=9), CASPR1 and the
400 extracellular matrix protein tenascin-C were found to localise together in the calyceal junction area, as described
401 previously in rodent samples (Lysakowski et al., 2011; Sedó-Cabezón et al., 2015; Greguske et al., 2019). In
402 contrast, the observed label of HCI by SPP1 was unreliable in the tested conditions. Among the 29 epithelia, HC
403 densities varied from high, similar to that observed in samples from control rats, to almost null. Reduced HC
404 density could result from both the patient's age and vestibular pathology; the evaluation of this pathology was
405 beyond the scope of the present study. Regarding the calyceal junctions, 18 samples were evaluated to have
406 intact or mostly intact CASPR1-labelled calyces. These included 2/2 cases of Ménière's Disease (Fig. 8A), 4/4

407 cases of meningioma (Fig. 8B,C), 1/1 case of an endolymphatic sac tumour, and 11/22 cases of vestibular
408 schwannoma. Two other samples displayed very few HCs with only one CASPR1+ or none, hampering the
409 achievement of any conclusion on calyceal junctions. However, 9 of the samples, all of them from vestibular
410 schwannoma patients, provided images suggesting that an active process of calyceal junction dismantlement
411 was taking place. This included calyces with patched CASPR1 labelling (Fig 8D-F) or lack of CASPR1 in calyx-only
412 units (Fig. 8G). The patched feature of the label in some calyces was confirmed in 3D reconstructions (Suppl. Fig.
413 S8). The number of days the samples were in fixative does not explain this effect, as it was observed in tissues
414 fixed for 1 day (n=5), 4 days (n=1), 7 days (n=1), and unrecorded (but less than 8) days (n=2).

415 **DISCUSSION**

416 Previous work from our laboratory in rats and mice has demonstrated that sub-chronic IDPN exposure causes
417 vestibular HC extrusion and that the extrusion is preceded by reversible calyceal junction dismantlement and
418 synaptic uncoupling (Seoane et al., 2001a; Sedó-Cabezón et al., 2015; Greguske et al., 2019). These phenomena
419 have received little research attention despite its potential relevance. HC extrusion is the main form of HC
420 demise in birds and amphibians (Hirose et al., 1999; Rubel et al., 2013) and has been sporadically observed in
421 mammalian vestibular epithelia (Li et al., 1995; Nakagawa et al., 1997; Granados and Meza, 2005). In the present
422 work, we first aimed at establishing a new rat model of sub-chronic aminoglycoside toxicity to determine
423 whether HC detachment and extrusion occur in ototoxic conditions of clinical relevance. The data obtained
424 demonstrate that the calyceal junction reversibly dismantles during subchronic streptomycin exposure in
425 association with reversible vestibular dysfunction. Synaptic uncoupling and HC extrusion were also recorded in
426 these rats. In addition, we also collected evidence indicating that calyceal junction dismantlement may take
427 place in the human vestibular system.

428 HC degeneration is effectively achieved by direct exposure to aminoglycoside antibiotics as done by trans-
429 tympanic administration or in *in vitro* studies (Kohonen and Tarkkanen, 1969; Anniko et al., 1982). However, the
430 use of more natural *in vivo* approaches to induce inner ear toxicity in laboratory animals with aminoglycosides
431 has been a challenging issue, as acute systemic intoxication may not cause ototoxic effects until the dose is large
432 enough to trigger animal death (Wu et al., 2001; Murillo-Cuesta et al., 2010). Nevertheless, several studies have
433 succeeded in establishing dosing regimes that elicit ototoxic effects with limited lethality and systemic toxicity.
434 Yet, many of these studies favour cochlear versus vestibular toxicity (Sullivan et al., 1987) or are designed to
435 accelerate the progression of the damage (Taylor et al., 2008; Oesterle et al., 2008). In the present study, we
436 successfully caused slowly progressing vestibular toxicity with streptomycin in young rats. By means of one daily
437 injection, significant loss of vestibular function occurred after four weeks of the highest tolerated dose, while
438 the use of two injections per day accelerated this loss in a dose-dependent manner, allowing for the study of

439 ototoxicity emerging after 2-3 weeks of treatment. Interestingly, the effects were similar in both sexes and low
440 variability was recorded within groups. Thus, as similarly reported for cochlear kanamycin toxicity in rats and
441 mice (Wu et al., 2001; Jiang et al., 2006), exposure of Long-Evans rats to one or two daily doses of streptomycin
442 reliably causes vestibular toxicity. Comparing the two models, it appears that the one daily dose regimen
443 reaches a limit in its effect, while the two-dose regimen seems to provide a more flexible model to study dose-
444 and time-dependent effects.

445 Streptomycin exposure in rats caused the loss of HCs, deeper after two daily doses than after one dose, as
446 revealed by the SEM studies and quantified in immunofluorescence studies. Separate counts of HCI and HCII
447 revealed that HC loss concentrated on the HCI, while HCII were spared in both injection paradigms. To identify
448 HCI we used two different markers, CASPR1 and SPP1. CASPR1 is not expressed by HCIs but is found in the
449 membrane of the calyx afferent contacting the HCI (Sousa et al., 2009; Lysakowski et al., 2011; Sedó-Cabezón et
450 al., 2015). Although streptomycin caused a specific loss of CASPR1, traces of CASPR1 label in contact with cell
451 profiles positive for Myo7a+ and negative for calretinin (see Fig 3A) allowed a reliable identification of HCI in the
452 one dose samples. Also, except for a minor recuperation in HCI numbers in the periphery of utricles and cristae,
453 no increase in HCI numbers was found in the samples of the recovery animals, in which a good recuperation in
454 CASPR1 expression had occurred. In addition, the loss of HCI was confirmed using a positive HCI marker, SPP1
455 (McInturff et al., 2018), to evaluate the samples from the two daily injections experiment. To identify HCII, we
456 also used a positive marker, calretinin, and found that the number of HCII per image was not reduced in any of
457 the two exposure paradigms. Because of the method used, we cannot completely exclude that a small loss of
458 HCII was masked by tissue shrinkage, but in any case the lack of differences in HCII numbers per image contrasts
459 with the significant loss of HCI. While a greater sensitivity of HCI with respect to HCII in regards to ototoxic insult
460 is widely recognized, not many studies are available in providing a quantitative assessment of this difference *in*
461 *vivo* (Lopez et al., 1997; Nakayama et al., 1996 ; Hirvonen et al., 2005; Maroto et al., 2021a).

462 The data collected add to the existing evidence that HC extrusion is a significant form of HC demise induced by
463 aminoglycosides in the mammalian vestibular system *in vivo*, as reported in the vestibular epithelia of rodents
464 exposed to other aminoglycosides using relatively long exposure paradigms (Li et al., 1995; Granados and Meza,
465 2005). Also, the present data demonstrate that calyceal junction dismantlement and synaptic uncoupling occur
466 after streptomycin, as previously demonstrated for sub-chronic IDPN (Sedó-Cabezón et al., 2015; Greguske et
467 al., 2019). The streptomycin effect includes CASPR1 down-regulation, redistribution of KCNQ4, loss of electron
468 density in the calyceal junction area, and a reduction in the number of synaptic puncta per cell. As observed in
469 the IDPN model, these effects are associated with the loss of vestibular function, and significant recuperation
470 was also recorded for the behavioural, CASPR1, and KCNQ4 effects in rats when allowed a recovery period after
471 the exposure. However, significant differences between the two models were noticed. In the rat IDPN model
472 (Seoane et al., 2001a; Sedó-Cabezón et al., 2015), a complete dismantlement of the calyceal junctions, with
473 extensive loss of CASPR1 and redistribution of KCNQ4 occurs before HC loss starts. Extending the time of IDPN
474 exposure triggers a massive event of HC extrusion, and the occurrence of extruding cells over several weeks
475 indicates that the extrusion of each HC takes place over several days. IDPN thus provides a highly synchronic and
476 slowly progressing model of sequential HC detachment and extrusion. In contrast, in the streptomycin rats,
477 extruding HC were only found occasionally, the loss of CASPR1 and the redistribution of KCNQ4 were smaller,
478 and a significant loss of HCs had occurred already before complete dismantlement of the calyceal junctions.
479 These observations indicate that, in comparison to those of IDPN, the effects of streptomycin are less
480 synchronic, and that the extrusion of each HC takes place in a shorter time, probably a few hours. Although not
481 specifically addressed in the present experiments, the TEM studies did not give evidence for an extensive
482 occurrence of apoptotic HC death. The simplest explanation of the present observations is that HC detachment
483 and extrusion are triggered at the individual cell level, and that cells are not synchronized after streptomycin
484 treatment as they are after IDPN. This conclusion is supported by our previous demonstration that calyceal

485 junction dismantlement is triggered individually in a calyx-to-calyx basis also after IDPN (Sedó-Cabezón et al.,
486 2015).

487 Behavioural and CASPR1 data presented here demonstrate repair capacity and functional recuperation of the rat
488 vestibular epithelium after sub-chronic streptomycin exposure. Although only a limited number of animals were
489 allowed to survive, their recuperation was indubitable. Functional recuperation may be a consequence of
490 behavioural compensation or reflect recuperation from alterations not detected by histological analyses, such as
491 hypothetical changes in endolymph composition or inactivation of the transduction channels. Conversely, our
492 data excluded the possibility that HC regeneration accounted for this recuperation, because HCI counts
493 remained decreased at the end of the recovery period. Rather, its association with the reversal in CASPR1
494 labelling, as measured on a cell-by-cell basis, suggests that the functional recuperation may result, at least in
495 part, from repair phenomena in the HC and the contact between HCs and their afferents. The present
496 observation of a recuperation in CASPR1 labelling contradicts the persistence of calyceal pathology observed in
497 chinchillas exposed to gentamicin by direct perilymphatic infusion (Sultemeier and Hoffman, 2017). Differences
498 in species, aminoglycosides, and exposure model may account for the difference between the present data and
499 those by Sultemeier and Hoffman (2017).

500 To explore the possible relevance of the calyceal junction dismantlement to human pathology, we examined a
501 series of human samples for histological evidence of such dismantlement. The interpretation of the human
502 observations is weakened by the lack of control samples, and the variability in pathological conditions and
503 surgery-generated damages. Nevertheless, many samples included a uniform CASPR1 label in all observable
504 calyces, while some other samples offered multiple images of patched or largely missing label for this protein.
505 Although the possibility that this abnormality was generated during collection of the sample cannot be
506 completely excluded, the data strongly suggest that calyceal junction dismantlement may indeed occur in the
507 human vestibule under stressful conditions. Although all the cases in which CASPR1 loss was recorded were
508 from vestibular schwannoma surgeries, the number of samples from other pathologies was so low that it cannot

509 be discarded that similar observations could emerge if more cases were examined. Current evidence indicates
510 that vestibular schwannomas may damage the sensory epithelia of the inner ear through tumour-secreted
511 factors, including tumour necrosis factor alpha (TNFα) (Dilwali et al., 2015). A recent study has demonstrated
512 the potential of this pro-inflammatory cytokine to cause cochlear synaptic uncoupling *in vivo* (Katsumi et al.,
513 2020). It is thus possible that inflammatory signals like TNFα are able to trigger the dismantlement of the
514 calyceal junction, synaptic uncoupling, and eventual HC extrusion in the vestibular epithelium.

515 Future work may address some of the limitations of this initiating study and use it to expand our understanding
516 of vestibular pathophysiology. For instance, determining the blood and inner ear concentrations of streptomycin
517 (and its potential ototoxic metabolites, e.g. Granados and Meza, 2005) in this exposure model may enlighten the
518 role of inner ear accumulation in systemic aminoglycoside toxicity. Recent data supports that cochlear retention
519 is a key factor in cisplatin ototoxicity (Breglio et al., 2017), and some data is available supporting a similar
520 conclusion for the cochlear and vestibular toxicity of gentamicin (Imamura and Adams, 2003). More works is
521 also needed to replicate and expand the human observations, excluding any potential confounding factor and
522 relating the pathological findings to the clinical data of patients. This is particularly important due to the lack of
523 tissues from humans not suffering any inner ear disease.

524 In conclusion, the present study evaluated whether events leading to HC extrusion in the vestibular sensory
525 epithelia of rodents exposed to sub-chronic IDPN (Seoane et al., 2001a; Sedó-Cabezón et al., 2015; Greguske et
526 al., 2019) may have a wider significance. The data collected demonstrate that dismantlement of the calyceal
527 junction and synaptic uncoupling are widespread phenomena in rats exposed to sub-chronic streptomycin
528 regimes that cause HC loss through, at least in part, the extrusion pathway. We also collected data suggesting
529 that calyceal junction dismantlement may occur in human vestibular epithelia in response to inflammatory
530 stress. Elucidating the molecular pathways triggering these cellular phenomena may unveil new targets to
531 control damage progression in this sensory epithelium.

532 **REFERENCES**

533 Anniko, M., Takada, A. and Schacht, J. (1982) Comparative ototoxicities of gentamicin and netilmicin in three
534 model systems. *Am. J. Otolaryngol.* 3, 422-33.

535 Beisel, K.W., Rocha-Sanchez, S.M., Morris, K.A., Nie, L., Feng, F., Kachar, B., Yamoah, E.N. and Fritzsch, B (2005)
536 Differential expression of KCNQ4 in inner hair cells and sensory neurons is the basis of progressive high-
537 frequency hearing loss. *J. Neurosci.* 25, 9285–9293.

538 Benkafadar, N., Janesick, A., Scheibinger, M., Ling, A. H., Jan, T. A. and Heller, S. (2021). Transcriptomic
539 characterization of dying hair cells in the avian cochlea. *Cell Rep.* 34, 108902. doi:
540 10.1016/j.celrep.2021.108902

541 Black, F.O., Gianna-Poulin, C. and Pesznecker, S.C. (2001). Recovery from vestibular ototoxicity. *Otol. Neurotol.*
542 22, 662-671.

543 Black, F.O., Pesznecker, S. and Stallings, V. (2004). Permanent gentamicin vestibulotoxicity. *Otol. Neurotol.* 25,
544 559-569.

545 Breglio, A. M., Rusheen, A. E., Shide, E. D., Fernandez, K. A., Spielbauer, K. K., McLachlin, K. M., Hall, M. D.,
546 Amable, L. and Cunningham, L. L. (2017). Cisplatin is retained in the cochlea indefinitely following
547 chemotherapy. *Nat. Commun.* 8, 1654.

548 Burns, J. C., Kelly, M. C., Hoa, M., Morell, R. J. and Kelley, M. W. (2015). Single-cell RNA-Seq resolves cellular
549 complexity in sensory organs from the neonatal inner ear. *Nat. Commun.* 6, 8557. doi:
550 10.1038/ncomms9557

551 Dechesne, C.J., Winsky, L., Kim, H.N., Goping, G., Vu, T.D., Wenthold, R.J. and Jacobowitz, D.M. (1991)
552 Identification and ultrastructural localization of a calretinin-like calcium-binding protein (protein 10) in the
553 guinea pig and rat inner ear. *Brain. Res.* 560, 139-148.

554 Dilwali, S., Landegger, L. D., Soares, V. Y., Deschler, D. G. and Stankovic, K. M. (2015). Secreted factors from
555 human vestibular schwannomas can cause cochlear damage. *Sci. Rep.* 5, 18599. doi: 10.1038/srep18599

556 Furness, D.N. (2015). Molecular basis of hair cell loss. *Cell Tissue Res.* 361, 387-399.

557 Granados, O. and Meza, G. (2005). Streptidine, a metabolic derivative produced after administration of
558 streptomycin in vivo, is vestibulotoxic in rats. *Histol. Histopathol*. 20, 357-364.

559 Greguske, E.A., Carreres-Pons, M., Cutillas, B., Boadas-Vaello, P. and Llorens, J. (2019) Calyx junction
560 dismantlement and synaptic uncoupling precede hair cell extrusion in the vestibular sensory epithelium
561 during sub-chronic 3,3'-iminodipropionitrile ototoxicity in the mouse. *Arch. Toxicol.* 93, 417-434.

562 Hasson, T., Gillespie, P.G., Garcia, J.A., MacDonald, R.B., Zhao, Y., Yee, A.G., Mooseker, M.S., Corey, D.P. (1997)
563 Unconventional myosins in inner-ear sensory epithelia. *J. Cell. Biol.* 137, 1287-1307.

564 Hirose, K., Westrum, L.E., Stone, J.S., Zirpel, L. and Rubel, E.W. (1999) Dynamic studies of ototoxicity in mature
565 avian auditory epithelium. *Ann. N.Y. Acad. Sci*. 884, 389-409.

566 Hirvonen, T.P., Minor, L.B., Hullar, T.E. and Carey, J.P. (2005). Effects of intratympanic gentamicin on vestibular
567 afferents and hair cells in the chinchilla. *J. Neurophysiol*. 93, 643-655.

568 Hunt, M.A., Miller, S.W., Nielson, H.C. and Horn, K.M. (1987) Intratympanic injections of sodium arsanilate
569 (atoxil) solution results in postural changes consistent with changes described for labyrinthectomized rats.
570 *Behav. Neurosci.* 101, 427–428.

571 Imamura, S., and Adams, J.C. (2003) Distribution of gentamicin in the guinea pig inner ear after local or systemic
572 application. *J. Assoc. Res. Otolaryngol.* 4, 176-195.

573 Jiang, H., Sha, S. H., Forge, A. and Schacht, J. (2006). Caspase-independent pathways of hair cell death induced
574 by kanamycin in vivo. *Cell Death Differ.* 13, 20–30.

575 Katsumi, S., Sahin, M. I., Lewis, R. M., Iyer, J. S., Landegger, L. D., & Stankovic, K. M. (2020). Intracochlear
576 perfusion of tumor necrosis factor-alpha induces sensorineural hearing loss and synaptic degeneration in
577 guinea pigs. *Front. Neurol.* 10, 1353.

578 Kohonen, A. and Tarkkanen, J. (1969) Cochlear damage from ototoxic antibiotics by intratympanic application.
579 *Acta Otolaryngol.* 68, 90-97.

580 Li, L., Nevill, G. and Forge, A. (1995). Two modes of hair cell loss from the vestibular sensory epithelia of the
581 guinea pig inner ear. *J. Comp. Neurol*. 355, 405-417.

582 Llorens, J. and Rodríguez-Farré, E. (1997). Comparison of behavioral, vestibular, and axonal effects of subchronic
583 IDPN in the rat. *Neurotoxicol. Teratol*. 19, 117-127.

584 Llorens, J., Demêmes, D. and Sans, A. (1993). The behavioral syndrome caused by 3,3'-iminodipropionitrile and
585 related nitriles in the rat is associated with degeneration of the vestibular sensory hair cells. *Toxicol. Appl.*
586 *Pharmacol.* 123, 199-210.

587 Lopez, I., Honrubia, V., Lee, S.C., Schoeman, G. and Beykirch, K. (1997) Quantification of the process of hair cell
588 loss and recovery in the chinchilla crista ampullaris after gentamicin treatment. *Int. J. Dev. Neurosci.* 15,
589 447-461.

590 Lopez-Escamez, J.A., Carey, J., Chung, W.H., Goebel, J.A., Magnusson, M., Mandala, M., Newman-Toker, D.E.,
591 Strupp, M., Suzuki, M., Trabalzini, F. and Bisdorff, A. (2015) Diagnostic criteria for Menière's disease. *J.*
592 *Vestib. Res.* 25, 1-7.

593 Lysakowski, A., Gaboyard-Niay, S., Calin-Jageman, I., Chatlani, S., Price, S.D. and Eatock, R.A. (2011). Molecular
594 microdomains in a sensory terminal, the vestibular calyx ending. *J. Neurosci*. 31, 10101–10114.

595 Maroto, A. F., Barrallo-Gimeno, A. and Llorens, J. (2021a). Relationship between vestibular hair cell loss and
596 deficits in two anti-gravity reflexes in the rat. Hear. Res. 410, 108336. doi: 10.1016/j.heares.2021.108336

597 Maroto, A.F., Greguske, E.A., Barrallo-Gimeno, A. and Llorens, J. (2021b) Evaluation of cellular and molecular
598 pathology in the rodent vestibular sensory epithelia by immunofluorescent staining and confocal
599 microscopy. In: E*xperimental Neurotoxicology Methods, Neuromethods, vol. 172*, Llorens, J. and Barenys.
600 M., Editors. Springer US, pp 35-50.

601 Maroto, A.F., Greguske, E.A., Deulofeu, M., Boadas-Vaello, P. and Llorens, J. (2021c) Behavioral assessment of
602 vestibular dysfunction in rats. In: E*xperimental Neurotoxicology Methods, Neuromethods, vol. 172*, Llorens,
603 J. and Barenys. M., Editors. Springer US, pp 199-215.

604 Martins-Lopes, V., Bellmunt, A., Greguske, E.A., Maroto, A.F., Boadas-Vaello, P. and Llorens, J. (2019)
605 Quantitative assessment of anti-gravity reflexes to evaluate vestibular dysfunction in rats. *J. Assoc. Res.*
606 *Otolaryngol.* 20, 553-563.

607 McInturff, S., Burns, J.C., Kelley, M.W. (2018) Characterization of spatial and temporal development of Type I
608 and Type II hair cells in the mouse utricle using new cell-type-specific markers. *Biol. Open* 7, bio038083.
609 doi: 10.1242/bio.038083.

610 Murillo-Cuesta, S., Contreras, J., Cediel, R. and Varela-Nieto, I. (2010) Comparison of different aminoglycoside
611 antibiotic treatments to refine ototoxicity studies in adult mice. *Lab. Anim.* 44, 124-131.

612 Nakagawa, T., Yamane, H., Shibata, S. and Nakai, Y. (1997) Gentamicin ototoxicity induced apoptosis of the
613 vestibular hair cells of guinea pigs. *Eur. Arch. Otorhinolaryngol.* 254, 9-14.

614 Nakayama, M., Riggs, L.C. and Matz, G.J. (1996) Quantitative study of vestibulotoxicity induced by gentamicin or
615 cisplatin in the guinea pig. *Laryngoscope* 106, 162-167.

616 Oesterle, E.C., Campbell, S., Taylor, R.R., Forge, A. and Hume, C.R. (2008) Sox2 and JAGGED1 expression in
617 normal and drug-damaged adult mouse inner ear. *J. Assoc. Res. Otolaryngol.* 9, 65-89.

618 Pellis, S.M., Pellis, V.C. and Teitelbaum, P. (1991) Labyrinthine and other supraspinal inhibitory controls over
619 head-and-body ventroflexion. *Behav. Brain Res*. 46, 99-102.

620 Rubel, E.W., Furrer, S.A. and Stone, J.S. (2013). A brief history of hair cell regeneration research and speculations
621 on the future. *Hear Res*. 297, 42-51.

622 Schirmer, M., Kaiser, A., Lessenich, A., Lindemann, S., Fedrowitz, M., Gernert, M. and Löscher, W. (2007).
623 Auditory and vestibular defects and behavioral alterations after neonatal administration of streptomycin to
624 Lewis rats: Similarities and differences to the circling (ci2/ci2) Lewis rat mutant. *Brain Res*. 1155, 179–195.

625 Sedó-Cabezón, L., Jedynak, P., Boadas-Vaello, P. and Llorens, J. (2015) Transient alteration of the vestibular
626 calyceal junction and synapse in response to chronic ototoxic insult in rats. *Dis. Model. Mech.* 8, 1323-1337.

627 Seoane, A., Demêmes, D. and Llorens, J. (2001a). Relationship between insult intensity and mode of hair cell loss
628 in the vestibular system of rats exposed to 3,3'-iminodipropionitrile. *J. Comp. Neurol.* 439, 385-399.

629 Seoane, A., Demêmes, D. and Llorens, J. (2001b). Pathology of the rat vestibular sensory epithelia during
630 subchronic 3,3'-iminodipropionitrile exposure: hair cells may not be the primary target of toxicity. *Acta*
631 *Neuropathol*. 102, 339-348.

632 Sousa, A.D., Andrade, L.R., Salles, F.T., Pillai, A.M., Buttermore, E.D., Bhat, M.A. and Kachar, B (2009). The
633 septate junction protein caspr is required for structural support and retention of KCNQ4 at calyceal synapses
634 of vestibular hair cells. *J. Neurosci*. 29, 3103-3108.

635 Sullivan, M. J., Rarey, K. E. and Conolly, R. B. (1987). Comparative ototoxicity of gentamicin in the guinea pig and
636 two strains of rats. Hear. Res. 31, 161–167.

637 Sultemeier, D. R. and Hoffman, L. F. (2017). Partial aminoglycoside lesions in vestibular epithelia reveal broad
638 sensory dysfunction associated with modest hair cell loss and afferent calyx retraction. Front. Cell. Neuorsci.
639 11, 331.

640 Taylor, R.R., Nevill, G. and Forge, A. (2008) Rapid hair cell loss: a mouse model for cochlear lesions. *J. Assoc. Res.*
641 *Otolaryngol.* 9, 44-64.

642 von Brevern, M., Bertholon, P., Brandt, T., Fife, T., Imai, T., Nuti, D. and Newman-Toker, D. (2015) Benign
643 paroxysmal positional vertigo: Diagnostic criteria. *J. Vestib. Res.* 25, 105-117-

644 Wu, W.J., Sha, S.H., McLaren, J.D., Kawamoto, K., Raphael, Y. and Schacht, J. (2001) Aminoglycoside ototoxicity
645 in adult CBA, C57BL and BALB mice and the Sprague-Dawley rat. *Hear. Res.* 158; 165-178.

646 LEGENDS FOR FIGURES

647 **Figure 1.** Effects of sub-chronic streptomycin on the tail-lift reflex of rats. Data are mean ± SE minimum angles
648 formed by the nose, the back of the neck, and the base of the tail during the reflex behaviour elicited by a tail-
649 lift manoeuvre. Loss of vestibular function causes loss of the anti-gravity trunk extension reflex, which results in
650 ventral curling and thus in smaller angles. **A.** Effects of one injection per day at 0 (CTRL, vehicle control) or 500
651 mg/kg (STR-500) of streptomycin for 6 weeks, starting at 21 days of age. * $p<0.05$, different from control group
652 after significant day by treatment interaction effect in repeated-measures MANOVA. **B.** Effects of two injections
653 per day at 0 (CTRL, vehicle control), 300 (STR-300x2), 350 (STR-350x2), or 400 (STR-400x2) mg/kg of
654 streptomycin for 6, 6, 4, or 3 weeks, respectively, starting at 21 days of age. The numbers of animals were
655 reduced to 6 in the CTRL group after day 28, and to 7 in the STR-300x2 and STR-350x2 groups after day 21. **a, b,**
656 **c, d**: groups with different letters are significantly different ($p<0.05$), Duncan's test after significant ANOVA on
657 that day. **C.** Recuperation of the tail-lift reflex after the end of exposure in rats administered once a day with 500
658 mg/kg (STR-500) of streptomycin for 6 weeks. **D.** Loss and recuperation of the tail-lift reflex in two individual rats
659 administered twice a day with 350 (STR-350) or 400 mg/kg (STR-400) of streptomycin for 3 weeks, followed by 3
660 weeks of recovery.

661 **Figure 2.** Effects of sub-chronic streptomycin on the vestibular sensory epithelium of the rat as observed in
662 surface preparations of saccules examined by SEM. **A.** Control saccule, showing a high and uniform density of
663 stereocilia bundles throughout the macula. **B.** Effect of one injection per day of 500 mg/kg of streptomycin (STR-
664 500) for 8 weeks. A reduced density of stereocilia bundles is noticeable at this low magnification. The boxed area
665 is shown at higher magnification in panel C. **C.** Higher magnification of the saccule shown in panel B. Note the
666 areas where the lack of stereocilia bundles is evident (arrows). **D and E.** High magnification views of a saccule
667 from a STR-500 rat at 6 weeks of treatment. Note the contacts between the apical edges of supporting cells,
668 marked by a high density of microvellosities, denoting the lack of stereocilia bundles (star), and the bundles

669 showing stereocilia fusion and HC protrusion into the luminal cavity (arrows). **Scale Bars:** 100 μm in **A** and **B**; 20
670 μm in **C**; 2 μm in **D**; 5 μm in **E**.

671 **Figure 3.** Effect of sub-chronic streptomycin on the numbers of HCI and HCII in the vestibular epithelia of the rat.
672 **A, B, C**. Effect of 500 mg/kg of streptomycin, once a day, for 6 or 8 weeks, as recorded at the end of the
673 exposure period or at the end of a recovery period of 8 weeks after treatment. Vestibular cristae, utricles and
674 saccules were immunolabelled with anti-MYO7A (red, to label all HCs), anti-CASPR1 (green, to identify HCI) and
675 anti-calretinin (blue, to label HCII) antibodies, and examined by confocal microscopy. The central/striola and
676 peripheral regions of the epithelia were evaluated separately. **A**. Representative images from the peripheral
677 utricle of a vehicle control rat, a rat treated with streptomycin for 8 weeks (STR-500 8wk), and a recovery (STR-
678 500 R) rat. HCI were defined by MYO7A+ cells with adjacent CASPR1 label, even if thin or fragmented, and no
679 calterinin label (arrows). Note the fragmentation of the CASPR1 label in the STR-500 (8wk) rat. **Scale bar**: 20 μm.
680 **B and C.** Counts of HCI **(B)** and HCII **(C)** cells. Data are mean number of cells +/- SE per section. For each animal
681 and epithelial zone, numbers were obtained by averaging counts from 8 confocal stacks from a representative
682 histological section. **D, E**. Effect of 300 (STR-300x2), 350 (STR-350x2) or 400 (STR-400x2) mg/kg of streptomycin,
683 twice a day, for 6, 4, or 3 weeks. The recovery (R) group includes animals allowed 3 weeks of recovery after
684 receiving STR-350x2 or STR-400x2 for 3 or 4 weeks. Vestibular cristae were labelled with anti-SPP1 (blue, to label
685 HCI), anti-CASPR1 (green) and anti-calretinin (red) antibodies. HCI were defined as SPP1+ cells and HCII were
686 cells with calretinin label. **D.** Partial view of representative sections of control and streptomycin cristae. **Scale**
687 **bar**: 20 μm. **E.** Relative numbers of HCI and HCII in the crista sections. Data are mean number of cells +/- SE per
688 transversal section, including central and peripheral regions. In **B**, **C**, and **E**, the number of replicas in the figure
689 legends indicate minimum/maximum number of animals counted per epithelium and zone in the treatment
690 group. **a, b, c, ab**: groups not sharing a letter are different ($p<0.05$), Duncan's multiple-comparisons test after
691 significant ($p<0.05$) one-way ANOVA. **(n.s.):** non-significant ($p>0.05$) group differences in the ANOVA analysis.

692 **Figure 4.** Effects of sub-chronic streptomycin on the expression of CASPR1 in the central/striola (C/S) and
693 peripheral (P) regions of the vestibular crista, utricle and saccule of the rat. The samples were labelled with anti-
694 MYO7A (red), anti-CASPR1 (green) and anti-calretinin (blue) antibodies. **A.** Representative images from mid-
695 crista sections from a CTRL rat (**a** to **d**), a rat treated with 500 mg/kg of streptomycin, once a day, for 6 weeks (**e**
696 to **h**), and a rat allowed a recovery period of 10 weeks after the streptomycin treatment (**i** to **l**). Note the loss
697 and fragmentation of the CASPR1 label caused by streptomycin and its recuperation after recovery. The
698 intensity of MYO7A label also decreased and recovered. **B.** Quantitative analysis of the CASPR1 fluorescence.
699 Data are normalised arbitrary fluorescence amount per cell +/- SE. For each animal, epithelium and zone, the
700 average amount of fluorescence was obtained from all HCs available for analysis up to 40 cells. Numbers below
701 the bars indicate number of animals included per group. **a, b**: groups not sharing a letter are different ($p<0.05$),
702 Duncan's multiple-comparisons test after significant ($p<0.05$) one-way ANOVA.

703 **Figure 5.** Effects of sub-chronic streptomycin on the expression of synaptic proteins in the HCI and calyx
704 afferents of the rat. **A.** Redistribution of KCNQ4 in the inner and outer membranes of the calyx terminals
705 afferent to HCI. Vestibular crista from control (a1-a3) and streptomycin (a4-a6) animals are shown after labelling
706 with anti-CASPR1 (green) and anti-KCNQ4 (red) antibodies. Note the precise colocalization of CASPR1 and
707 KCNQ4 in the control epithelium. After streptomycin, KCNQ4 mislocalisation concurs with CASPR1 loss. The
708 asterisk indicates a calyx with a control-like co-localisation of CASPR1 and KCNQ4 in the inner membrane of the
709 calyx. The arrowhead points to a calyx with CASPR1 loss and reduced co-localisation, with the KCNQ4 antibody
710 labelling a greater area than the CASPR1 antibody. The arrow points to the outer membrane of a calyx displaying
711 greatly reduced CASPR1 label in the inner membrane and redistribution of KCNQ4 throughout both the inner (i
712 and i') and outer (o and o') membranes. **B.** Quantitative analysis of the distribution of KCNQ4 label in the inner
713 and outer face of the calyces in crista from control rats (CTRL), rats treated with 500 mg/kg of streptomycin
714 (STR-500), once a day, for 6 or 8 weeks, and rats allowed a recovery period of 8-10 weeks after the streptomycin
715 treatment. Note that control and recovery animals do not display KCNQ4 in the outer face membrane. Data are

716 mean arbitrary fluorescence units +/- SE. The number of replicas indicate the number of animals included in the
717 analysis per group. **a, b**: groups not sharing a letter are different ($p<0.05$), Duncan's multiple-comparisons test
718 after significant ($p<0.05$) one-way ANOVA. **C.** Labelling of pre-synaptic (Ribeye, red) and post-synaptic (PSD-95,
719 green) proteins on HCs (MYO7A, white) in vestibular crista. In subpanel **c1**, the MYO7A label is included to show
720 HC bodies in a control crista. Subpanel **c2** shows the same image without the MYO7A label but including lines
721 delineating the limits of two HCs and arrows pointing to examples of pairs of ribeye and PSD-95 puncta. **D.**
722 Effects of sub-chronic streptomycin on the numbers of synaptic puncta per 2.7 μm-tick optical sections of HCs.
723 Data are mean number of pre-synaptic and post-synaptic puncta, as well as pre- and post-synaptic pairs (Co-
724 localization), +/- SE, from control rats (CTRL) and rats treated with 500 mg/kg of streptomycin (STR-500), once a
725 day, for 6 weeks. The number of replicas indicate the number of animals included in the analysis per group. *: $p<$
726 0.05, and ***: $p<0.001$, CTRL versus STR-500, Student's T-test.

727 **Figure 6.** Effects of sub-chronic streptomycin on the calyceal junction and calyx integrity as observed by TEM. **A.**
728 Control crista. The calyceal junction is revealed by the high electron density of the apposing membranes (long
729 arrows) of HCI and inner side of the calyx (c), higher than that found in the outer side of the calyx (arrowheads).
730 **B.** Crista of a rat exposed to 500 mg/kg of streptomycin, once a day, for 6 weeks. In most of the area where the
731 calyceal junction should be found, the apposing membranes show a low electron density (short arrows), similar
732 to that in the outer face of the calyx (arrowhead). **C.** Higher magnification of the calyceal junction (long arrow)
733 and the outer side of the calyx (arrowhead) in a control saccule. **D.** Higher magnification from a crista of a rat
734 exposed to 500 mg/kg of streptomycin, once a day, for 6 weeks. Note the short segment of calyceal junction
735 (long arrow) that remains together with areas devoid of it (short arrow) and the similarity between the latter
736 and the membranes in the outer side of the calyx (arrowheads). **E.** Calyceal junction dismantlement and calyx
737 fragmentation in a HCI showing evidence of ongoing extrusion, from a utricle of a rat exposed to 300 mg/kg of
738 streptomycin, twice a day, for 6 weeks. Note the absence of calyceal junction (short arrows), the fragmentation
739 of the calyx (c, green shadow), and the direct contact between supporting cells and the HCI (stars). The purple

740 shadow highlights one supporting cell (sc). **F.** Higher magnification of the boxed area in panel **E**. Note the
741 similarity of the membranes between the place where the calyceal junction is missing (short arrows) and the
742 outer side of the calyx (arrowheads). Note also the direct contact between a supporting cell (sc) and the HCI
743 (star). **Scale Bars: A**, **B**, and **E**, 2 μm; **C**, **D**, and **F**, 1 μm.

744 **Figure 7.** Evidence of HC extrusion in utricles of rats exposed to sub-chronic streptomycin as observed by
745 immunofluorescence and TEM. The images are from rats administered twice a day with 350 mg/kg of
746 streptomycin for 4 weeks, or with 300 mg/kg for 6 weeks. **A.** Utricles immunolabelled with antibodies against
747 MYO7A (red), CASPR1 (green) and radixin (blue). The radixin label of stereocilia and microvilli outlines the
748 surface of the epithelium. Arrowheads point to HCs protruding (**a**, **b**), extruding (**c**, **d**, **e**) or completely extruded
749 (**f**) into the luminal cavity of the utricle. **B** and **C.** TEM images of HCs in a protrusion stage corresponding to that
750 shown in panels **a** and **b**, respectively, of part **A**. Stereocilia (arrows) and striated organelles (arrowheads)
751 identify the extruding cells as HCs. In **B**, note the position of the nucleus of the HC inside the epithelium, and the
752 remnant of a calyx terminal (green shadow) that identifies the HC as a HCI. In **C**, note the position of the nucleus
753 of the HC (unidentified type), half way into the luminal cavity of the utricle. **Scale Bars: A**, 20 μm; **B**, and **C**, 2 μm.

754 **Figure 8.** Evaluation of the calyceal junction in whole-mount vestibular epithelia from patients of vestibular
755 diseases, as revealed by CASPR1 immunolabel (green, light blue when co-localizing with calretinin blue label). In
756 the main panels, HC bodies are labelled with an anti-MYO7A antibody (red). Calretinin is shown in blue in main
757 panels **C** to **F**, and in purple in the inset in **C**. **A**. Epithelium from a patient of Ménière's Disease showing no
758 pathological features. Note the elevated density of HCs and the continuous distribution of the CASPR1 label
759 throughout the calyceal junction area of each HCI. **B.** Epithelium from a meningioma patient, showing also no
760 overt pathology. **C.** Epithelium from a meningioma patient. Note the low density of HCs and the normally
761 continuous CASPR1 label in calyces of both calretinin+ calyx-only terminals (arrowhead) and calretinin-
762 dimorphic terminals (short arrow). The **inset** displays the same two calyces; a thinner stack is shown to highlight

763 the uninterrupted CASPR1 label and its placement in the inner membrane of the calretinin+ calyx of the calyx-
764 only terminal. **D.** Utricle periphery from a vestibular schwannoma patient. Around different HCl, the calyceal
765 CASPR1 label is found in both normal continuous distribution (arrowhead) and in faint and broken distribution
766 (long arrows). **E.** Striola region of the same utricle in **D**. Although some calyceal junctions display a roughly
767 normal continuous distribution of the CASPR1 label (arrowheads), most display faint, broken or largely absent
768 label (arrows). **F**. Higher magnification image from the same patient in **D** and **E.** Two calyces formed by calyx-
769 only terminals are highlighted, one with continuous CASPR1 label (arrowhead) and the other with a patched
770 distribution of this label (long arrow). **G.** Epithelium from a different vestibular schwannoma patient displaying
771 normal CASPR1 distribution in calyces from dimorphic terminals (arrowhead) and a double calyx of a calretinin+
772 calyx-only terminal displaying a partial CASPR1 label in one HC (short arrow) and no CASPR1 in the other HC
773 (long arrow). **Image thickness: A**, 12 μm; **B**, 10 μm; **C**, main 9.5 μm, inset 5 μm; **D**, 1.6 μm; **E**, 2.6 μm; **F**, 5 μm; **G**,
774 6 μm. **Scale Bars: A**, **C**, **D**, and **E**, 25 μm; **B**, 50 μm; **F**, and **G**, 5 μm.

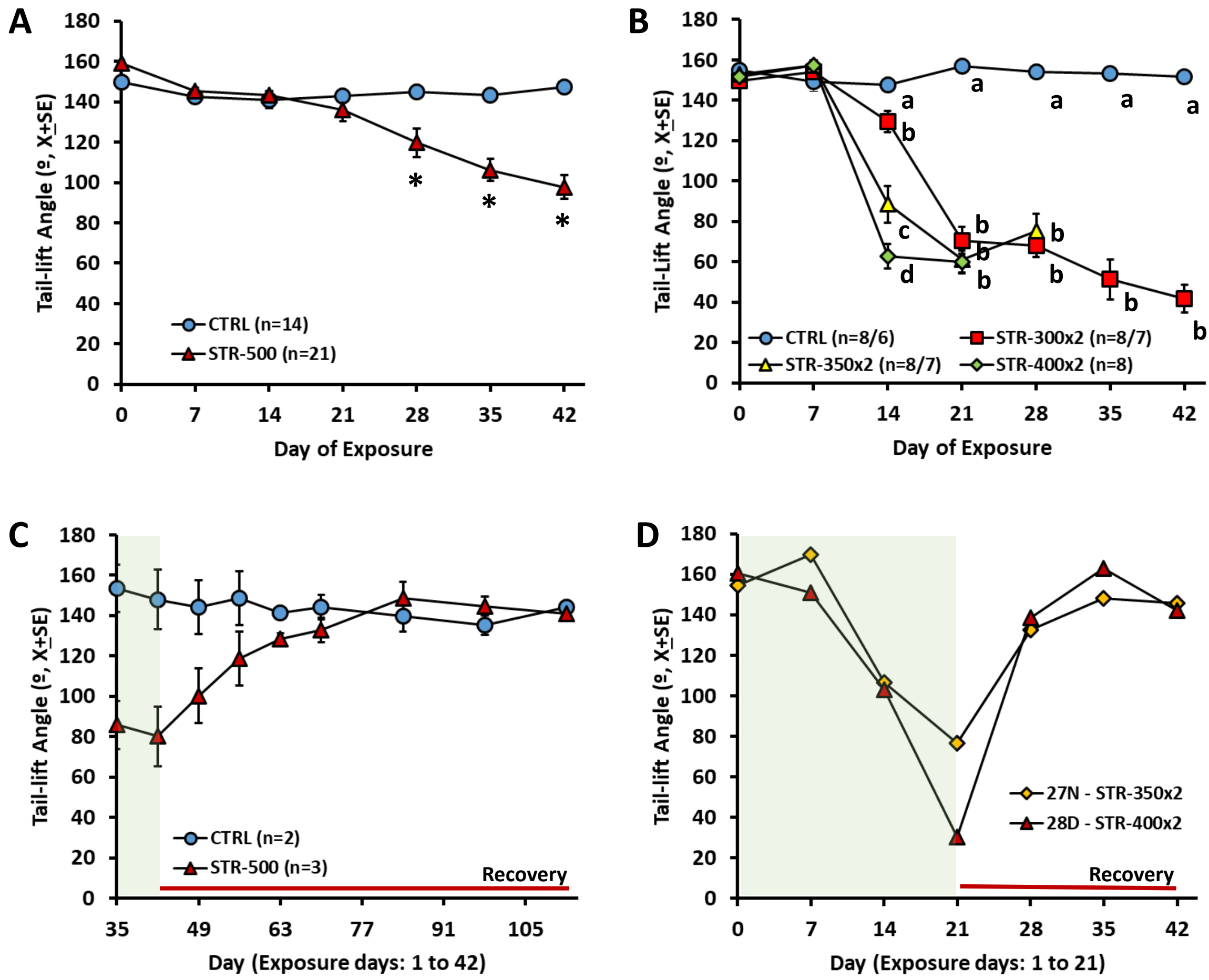
A
Tail-lift Angle (º, X+SE)
Day of Exposure
CTRL (n=14)
STR-500 (n=21)
B
Tail-Lift Angle (º, X+SE)
Day of Exposure
CTRL (n=8/6)
STR-300x2 (n=8/7)
STR-350x2 (n=8/7)
STR-400x2 (n=8)
C
Tail-lift Angle (º, X+SE)
Day (Exposure days: 1 to 42)
CTRL (n=2)
STR-500 (n=3)
Recovery
D
Tail-lift Angle (º, X+SE)
Day (Exposure days: 1 to 21)
27N - STR-350x2
28D - STR-400x2
Recovery

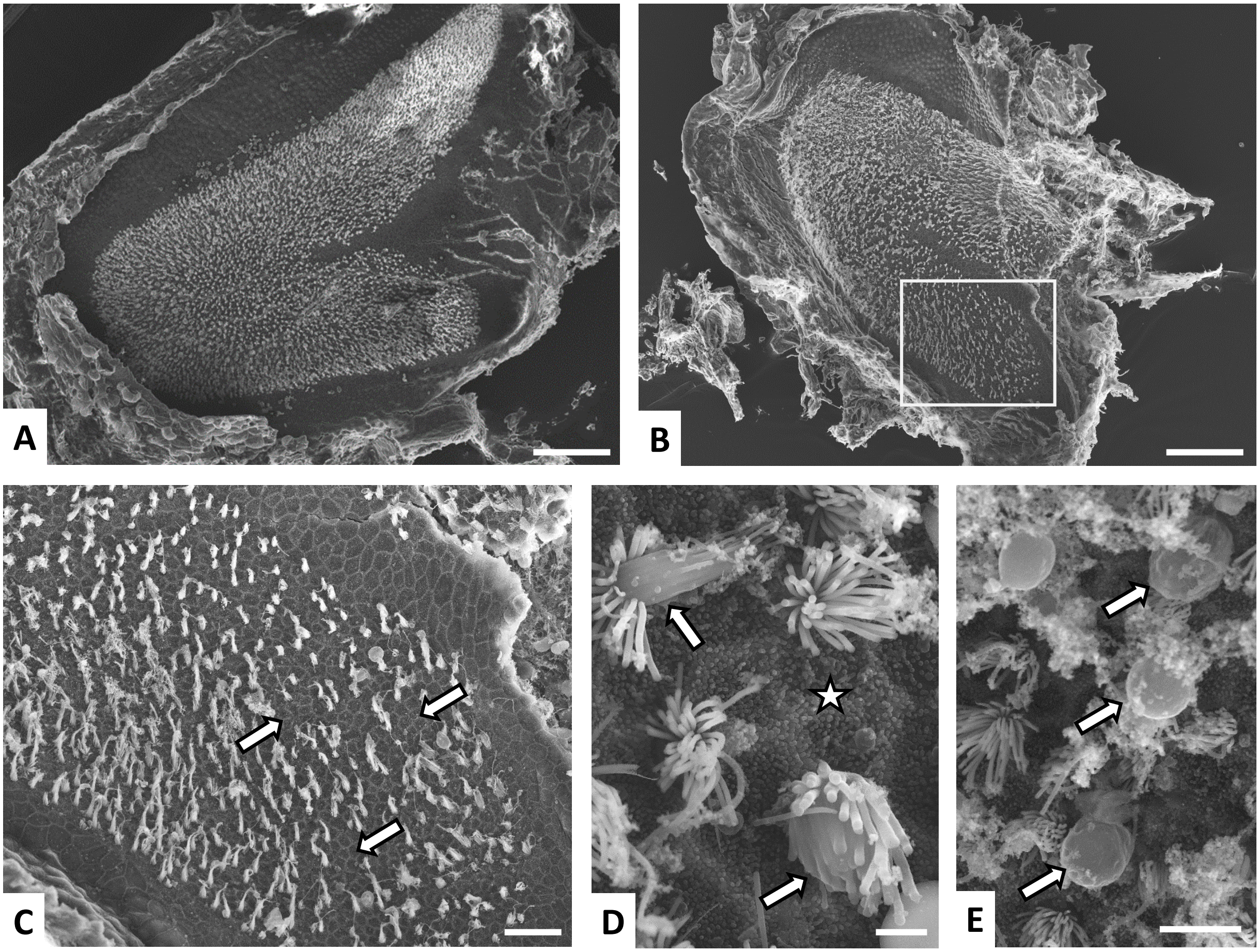
A
B
C
D
E

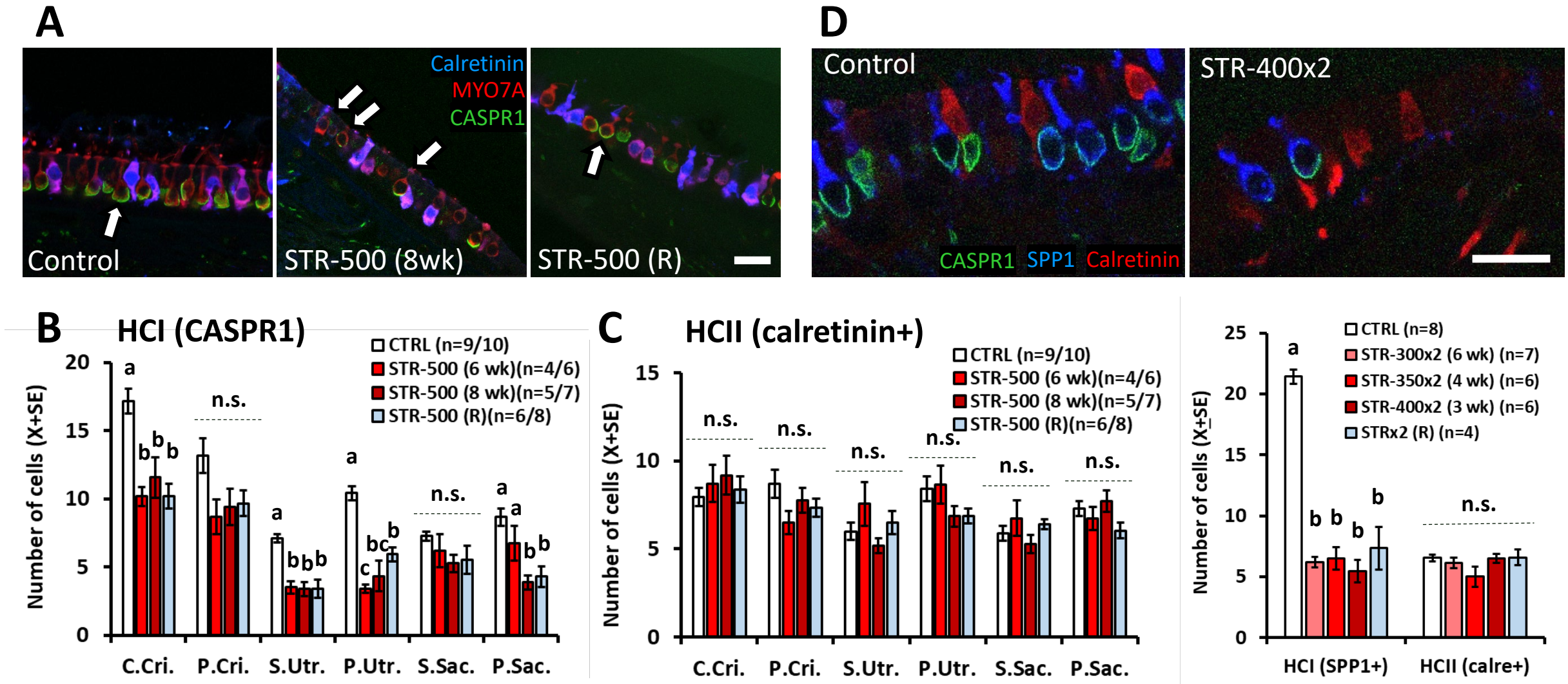
A
Calretinin
MYO7A
CASPR1
Control
STR-500 (8wk)
STR-500 (R)
D
Control
STR-400x2
CASPR1
SPP1
Calretinin
B
HCI (CASPR1)
CTRL (n=9/10)
STR-500 (6 wk)(n=4/6)
STR-500 (8 wk)(n=5/7)
STR-500 (R)(n=6/8)
Number of cells (X+SE)
n.s.
C.Cri.
P.Cri.
S.Utr.
P.Utr.
S.Sac.
P.Sac.
C
HCII (calretinin+)
CTRL (n=9/10)
STR-500 (6 wk)(n=4/6)
STR-500 (8 wk)(n=5/7)
STR-500 (R)(n=6/8)
Number of cells (X+SE)
n.s.
C.Cri.
P.Cri.
S.Utr.
P.Utr.
S.Sac.
P.Sac.
CTRL (n=8)
STR-300x2 (6 wk) (n=7)
STR-350x2 (4 wk) (n=6)
STR-400x2 (3 wk) (n=6)
STRx2 (R) (n=4)
Number of cells (X+SE)
HCI (SPP1+)
HCII (calre+)
n.s.

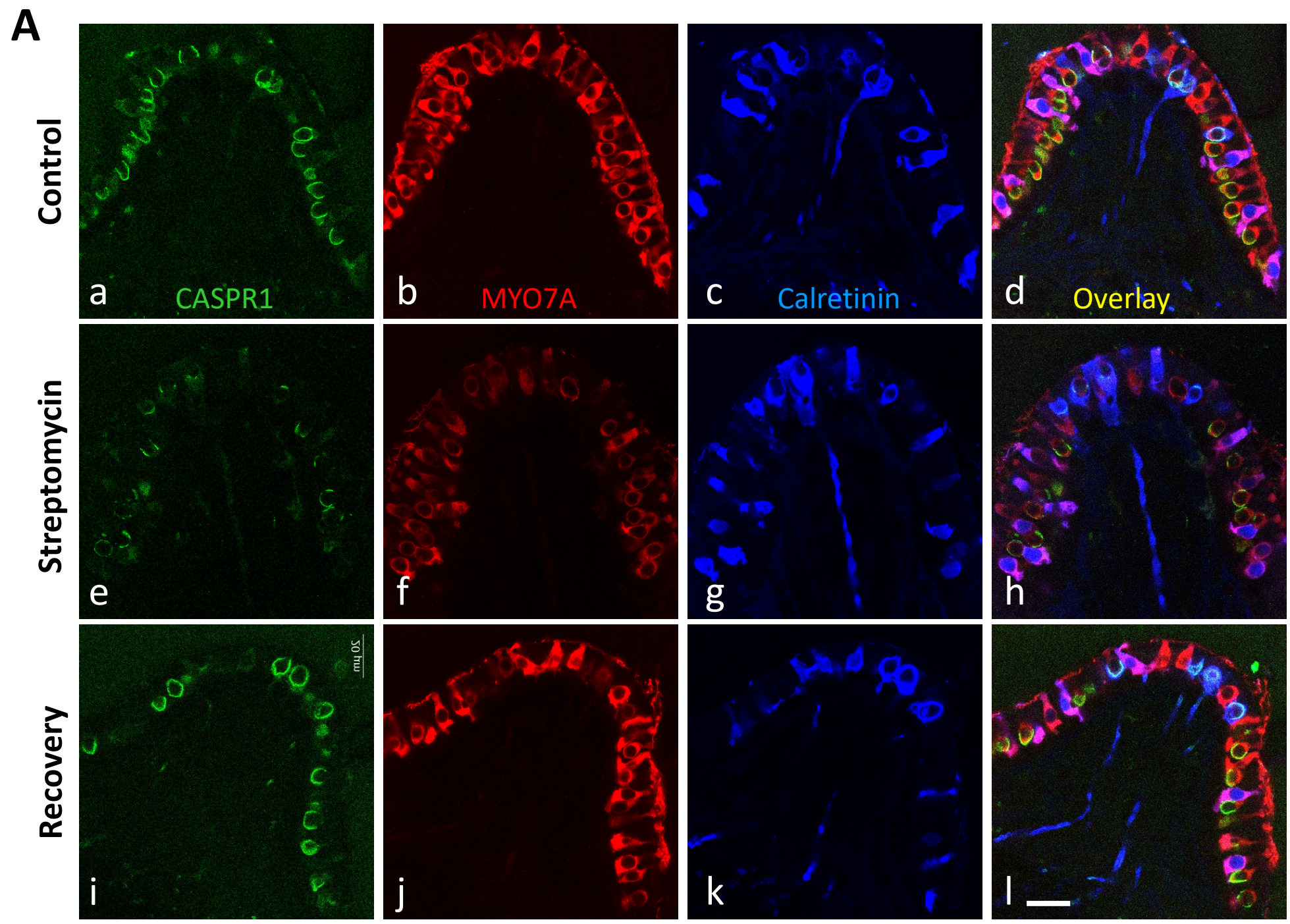
A
Control
Streptomycin
Recovery
a
CASPR1
b
MYO7A
c
Calretinin
d
Overlay
e
f
g
h
i
j
k
l
20 µm

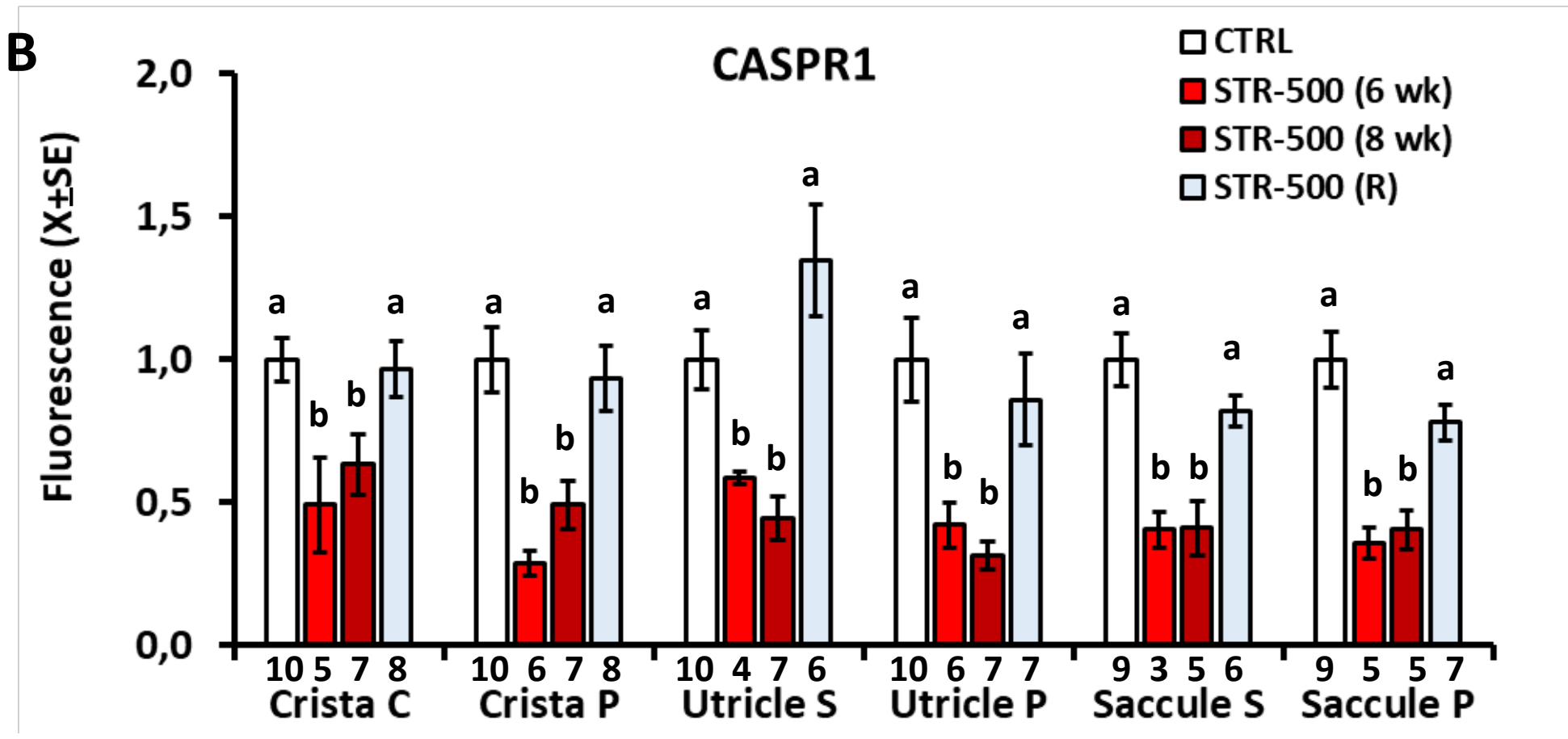
B
CASPR1
CTRL
STR-500 (6 wk)
STR-500 (8 wk)
STR-500 (R)
Fluorescence (X±SE)
2,0
1,5
1,0
0,5
0,0
10 5 7 8
10 6 7 8
10 4 7 6
10 6 7 7
9 3 5 6
9 5 5 7
Crista C
Crista P
Utricle S
Utricle P
Saccule S
Saccule P

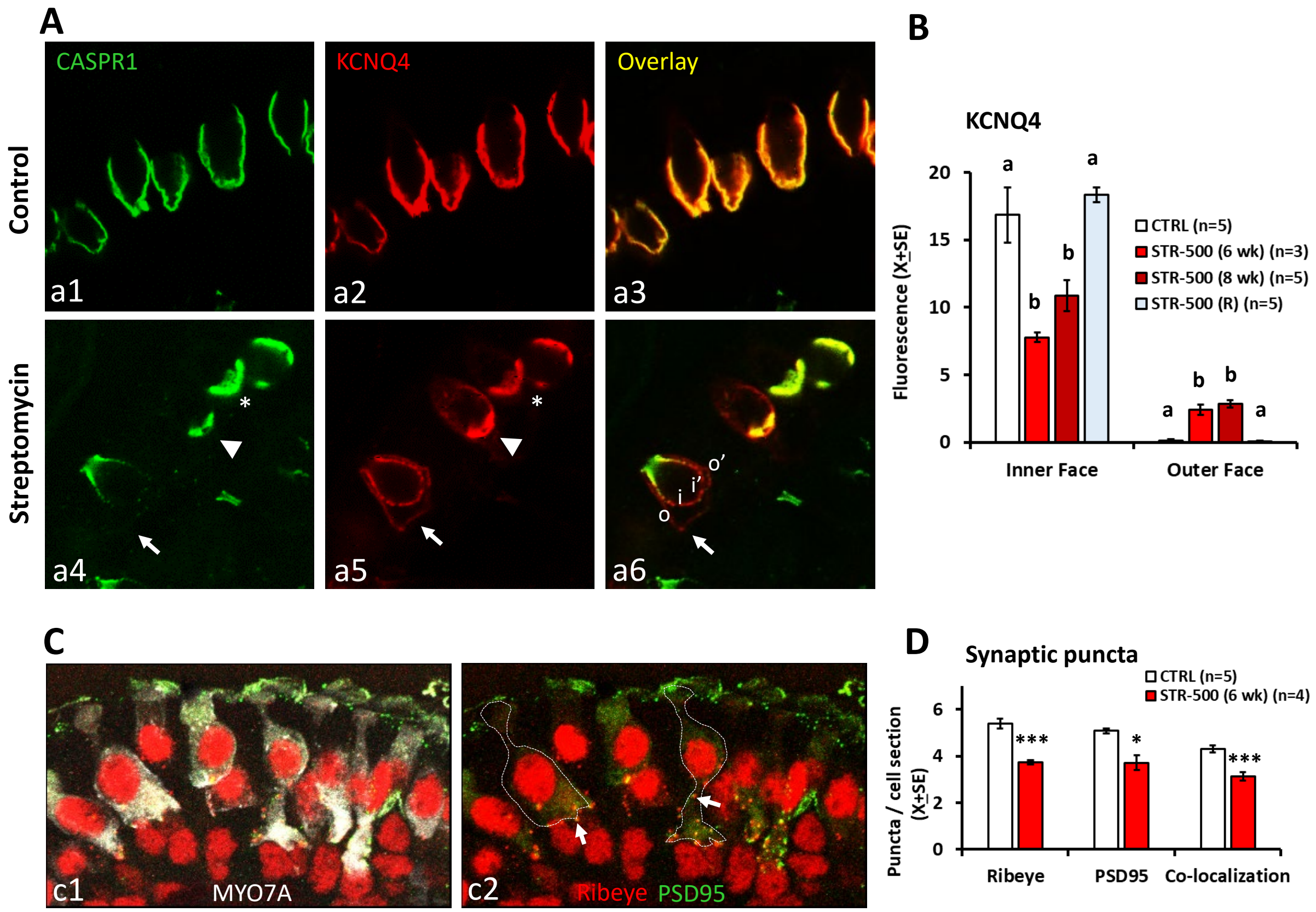
A
CASPR1
KCNQ4
Overlay
Control
Streptomycin
a1
a2
a3
a4
a5
a6
*
o
o'
i
i'
B
KCNQ4
Fluorescence (X±SE)
20
15
10
5
0
a
a
b
b
b
b
a
a
Inner Face
Outer Face
CTRL (n=5)
STR-500 (6 wk) (n=3)
STR-500 (8 wk) (n=5)
STR-500 (R) (n=5)
C
c1
MYO7A
c2
Ribeye PSD95
D
Synaptic puncta
CTRL (n=5)
STR-500 (6 wk) (n=4)
Puncta / cell section (X±SE)
6
4
2
0
***
*
***
Ribeye
PSD95
Co-localization

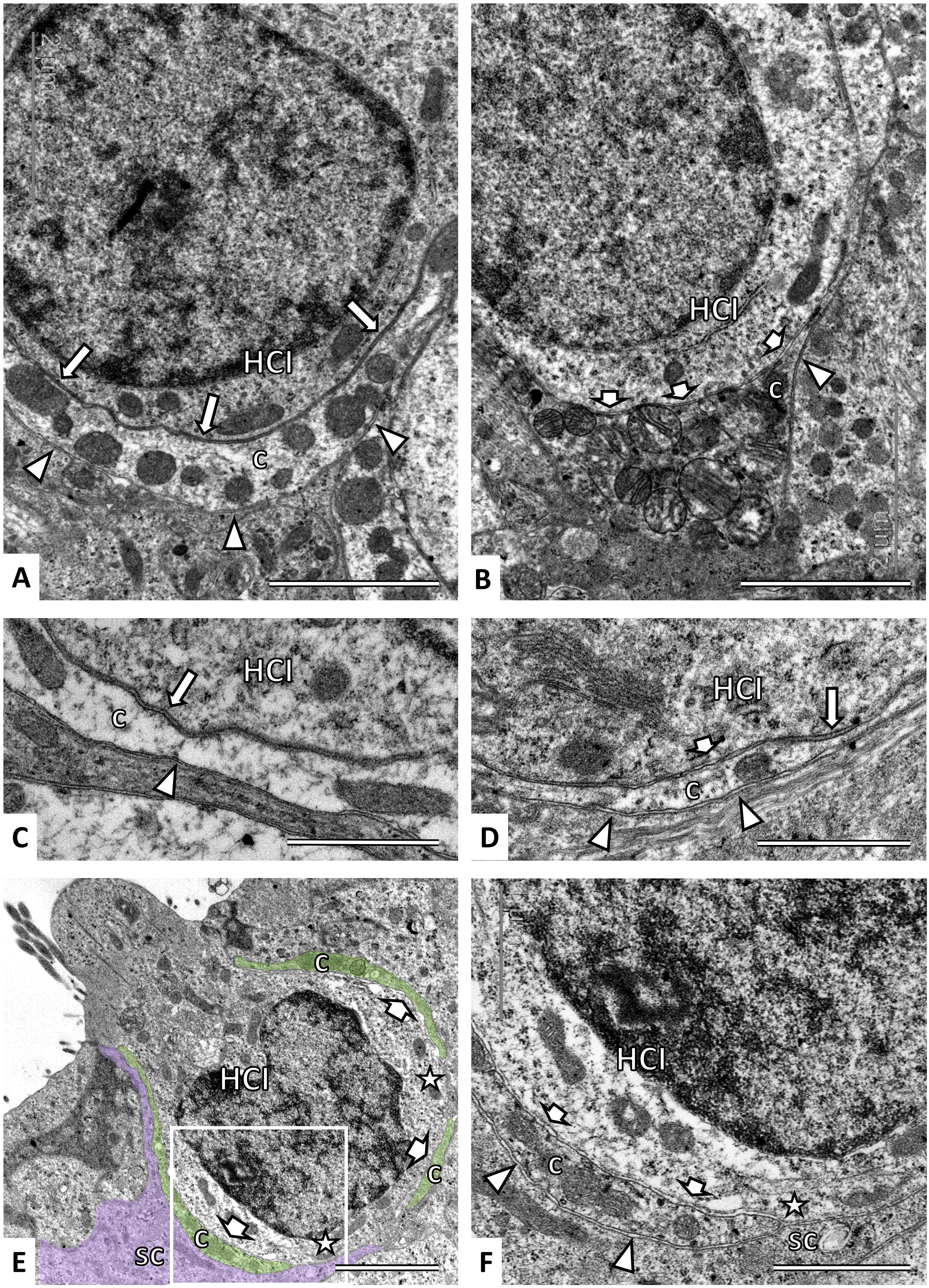
A
HCI
C
2 µm
B
HCI
C
2 µm
C
HCI
C
D
HCI
C
E
HCI
C
C
C
SC
F
HCI
C
SC

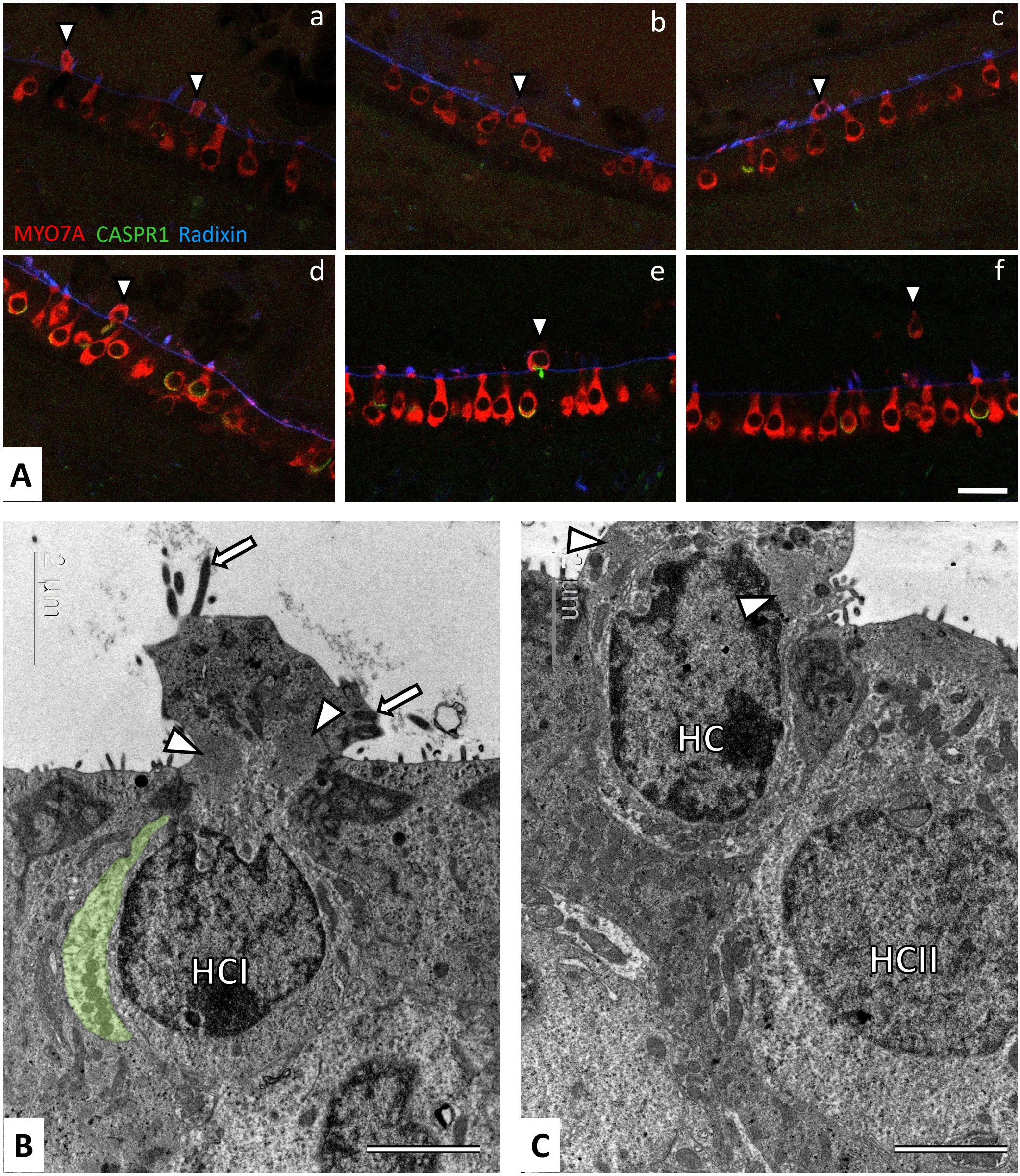
a
b
c
d
e
f
MYO7A CASPR1 Radixin
A
2 µm
HCI
B
3 µm
HC
HCII
C

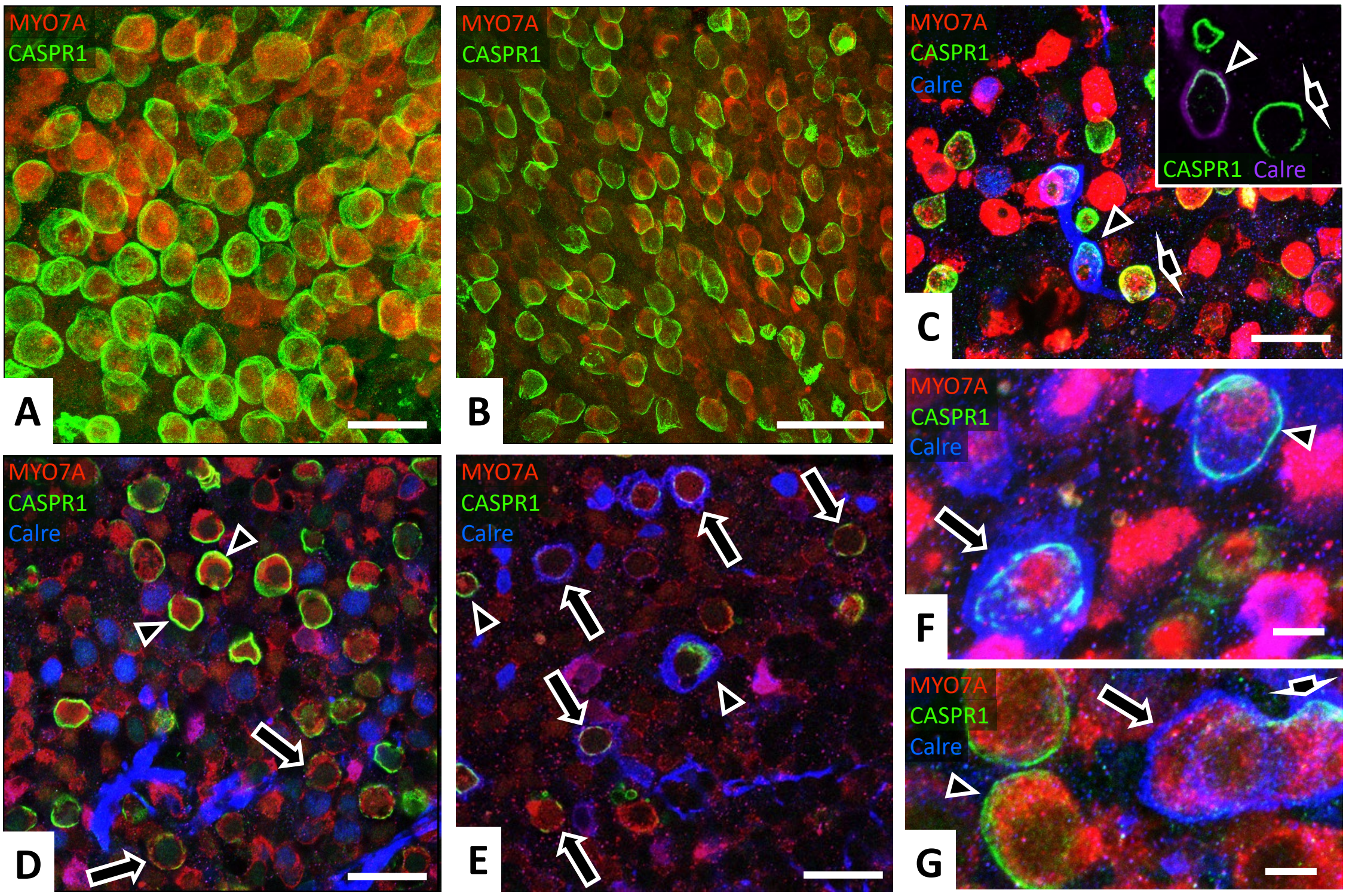
MYO7A
CASPR1
A
MYO7A
CASPR1
B
MYO7A
CASPR1
Calre
CASPR1 Calre
C
MYO7A
CASPR1
Calre
D
MYO7A
CASPR1
Calre
E
MYO7A
CASPR1
Calre
F
MYO7A
CASPR1
Calre
G